Catalysis Today 150 (2010) 279–299

Contents lists available at ScienceDirect

Catalysis Today

journal homepage: www.elsevier.com/locate/cattod

In-depth modeling of gas oil hydrotreating: From feedstock reconstruction to reactor stability analysis

C. López García *, D. Hudebine, J.-M. Schweitzer, J.J. Verstraete, D. Ferré

Institut Français du Pétrole, IFP Lyon, Process Development and Engineering Division, PO Box 3, 69360 Solaize, France

ARTICLE INFO

Article history:
Available online 19 September 2009

Keywords:
Gas oil hydrotreatment
Statistical reconstruction
Langmuir–Hinshelwood kinetic model
Dynamic reactor model
Thermal stability analysis

ABSTRACT

The increasing world demand for clean fuels requires improving existing hydrotreating (HDT) technologies through comprehensive studies of these complex reactive systems. This work presents an exhaustive modeling approach of diesel cut hydrotreating which ranges from the chemical characterization of gas oil feeds, over the HDT kinetic modeling and the thermal stability analysis of the reactor. In this approach, a "statistical reconstruction" method was developed to represent the composition by chemical family and by carbon number of different gas oils starting from a set of global analyses. A kinetic model based on a Langmuir–Hinshelwood representation was developed to determine the most adequate operating conditions to attain on-road diesel specifications, including sulfur levels as low as 10 wt ppm. Finally, since hydrotreating reactions are highly exothermic, the thermal stability analysis of a HDT reactor is also presented. This analysis consists of determining *a priori* whether the reactive system is thermally stable and therefore predicting if runaway will occur. For the latter, a complete dynamic model of the reactor was developed and used to assess the thermal runaway analysis by the perturbations theory.

© 2009 Elsevier B.V. All rights reserved.

1. Introduction

In recent years, the environmental constraints have become increasingly more severe, impacting both the quality and the maximum allowable amounts of impurities for commercial on-road fuels such as gasolines and diesels. For example, in the European Union (EU), the current legislation limits the total sulfur content to maximum 10 wt ppm. Hence, refiners face the challenge of producing ultra-low sulfur diesels (ULSD) while mainly using the existing classical technology: hydrotreating (HDT). Improved catalysts as well as a comprehensive knowledge of the reactivity of different gas oil feeds are therefore required to determine the most appropriate hydrotreatment conditions to meet commercial diesel specifications. In this work, we will focus on the modeling of the hydrotreating process.

When modeling gas oil hydrotreating, it is necessary to predict the HDT performances of the large variety of gas oils processed in refineries such as straight run gas oils (SR) obtained from direct crude oils distillation and gas oils obtained from conversion processes such as light cycle oils (LCO), and coker gas oils (CGO). The differences in reactivity obtained for such a variety of gas oils are obviously related to their dissimilar chemical composition. The different amounts and types of sulfur compounds, nitrogen compounds and hydrocarbons explain these reactivity differences for the various feeds. Hence, detailed characterization of these feeds is a key step for HDT modeling. Concerning the heteroatomic compounds, sulfur [1] and nitrogen speciation analyses are now relatively accessible techniques [2,3], generally based on gas chromatography with a specific elementary detector. Recent developments in two-dimensional gas chromatography (GC × GC) [4,5] allow to have access to detailed separation, identification and quantification of heteroatomic hydrocarbons. Concerning the major hydrocarbon families (saturates and aromatics), the molecular analysis and quantification remain impracticable, since gas oils are complex mixtures of hundreds or thousands of hydrocarbon species distributed over a large boiling point range. Even if there have been important analytical achievements in GC × GC for detailed hydrocarbon analysis in middle distillates

Abbreviations: BT, benzothiophenes; CARB, carbazoles; DBTs, dibenzothiophenes; DBT1, dibenzothiophenes in the highest reactivity lump; DBT2, dibenzothiophenes in the mid-reactivity lump; DBT3, dibenzothiophenes in the lowest reactivity lump; DI1, non-condensed diaromatics; DI2, condensed diaromatics; FBP, final boiling point (°C); IBP, initial boiling point (°C); IND, indoles; MONO, monoaromatics; NBAS, basic nitrogen compounds; PYRR, pyrroles; SAT, saturates family including paraffins and naphthenes; SULF, high reactivity sulfur compounds including mercaptans, sulfides, disulfides; TRI, triaromatics.

* Corresponding author. Tel.: +33 4 78 02 26 55; fax: +33 4 78 02 20 08.
E-mail addresses: clementina.lopez-garcia@ifp.fr (C. López García), damien.hudebine@ifp.fr (D. Hudebine), j-marc.schweitzer@ifp.fr (J.-M. Schweitzer), jan.verstraete@ifp.fr (J.J. Verstraete), daniel.ferre@ifp.fr (D. Ferré).

0920-5861/$ – see front matter © 2009 Elsevier B.V. All rights reserved.
doi:10.1016/j.cattod.2009.08.002

Nomenclature

Roman symbols

a	reaction order of hydrocarbon lump in the liquid phase
A	heat exchange surface (m^2/m^3)
b	reaction order of hydrogen in the liquid phase
C	concentration (mol/m^3)
C_p	specific heat capacity (J/kg/K)
D_{ax}	axial dispersion coefficient (m^2/s)
E	activation energy (J/mol)
$\vec{f}$	vector of the second member of partial differential equations
G	controller gain
H	Henry coefficient
h	heater height (m)
i	lump reference
j	reaction reference
$\mathbf{J}$	Jacobian matrix
K	adsorption equilibrium constant (L/mol)
k_0	reaction rate constant at the reference temperature
k_i	reaction rate constant (h^{-1}; $mol^{-1}\,L\,h^{-1}$; or $mol\,L^{-1}\,h^{-1}$)
L	length of side chain for statistical reconstruction
MW	molecular weight (g/mol)
nC_{alph}	number of aliphatic carbon atoms in the alkyl chains
N_{chains}	number of side chains for statistical reconstruction
nz	number of steps for the reactor discretization
P	pressure (bar)
P_t	total pressure (bar)
Q	electrical power (W)
Q_{gen}	heat generated by reactions (W)
Q_{trans}	heat transferred through the wall (W)
R	ideal gas constant (J/mol/K)
r	reaction rate ($mol/s/kg_{catalyst}$)
R	the universal gas constant (J/mol/K)
SimDist	simulated distillation ASTM D2887
S_r	reactor section surface (m^2)
S_{void}	section surface between the heaters and the reactor wall (m^2)
t	time (s)
T	temperature (K)
T_{amb}	ambient temperature (K)
T_b	pseudo-compound boiling point (K)
$T_{b,head}$	boiling point of the head of the family (K)
T_{ref}	reference temperature (K)
u	superficial liquid velocity (m/s)
U	heat transfer coefficient ($W/m^2/K$)
V_m^T	molar volume of the pseudo-compound at T (°C)
V	eigenvector
x	perturbation
$\vec{x}$	vector of perturbations
$\vec{y}$	variables vector
z	axial coordinate (m)

Greek symbols

α_j	LFER coefficient for reaction type, j
τ	hydrogenation site
σ	hydrogenolysis site
θ_τ	fraction of free τ sites
θ_σ	fraction of free σ sites
$\theta_{i\tau}$	fraction of lump i covering the τ sites
$\theta_{i\sigma}$	fraction of lump i covering the σ sites

Subscripts and superscripts

air	air between the reactor wall and the heater (K)
aliph	aliphatic
b	boiling point
C	cooling
g	gas
head	head of the corresponding family
heater	heater
i	hydrocarbon lump index
j	reaction index
k	number of heater index
l	liquid
loss	relative to heat loss
n	total number of variables/carbon number in the kinetic model
op	operating point
p	perturbed
por	porosity
s	solid
set	setpoint
steel	reactor steel
W	internal reactor thermowell
wall	reactor external wall

[6,7], allowing to arrive at a more detailed characterization of these cuts, these kind of analyses are not widespread. Indeed, the chemical characterizations commonly practiced are mainly the standardized methods, and most of the time, refiners limit themselves to those specified in the commercial diesel specifications such as density (ASTM D4052), simulated distillation (ASTM D2887) or UV aromatics (NF EN 12916). Molecular characterization is still extremely complex for most laboratories and remains therefore very rare. For that reason, a molecular reconstruction method termed "statistical reconstruction" was developed to overcome this lack of information, which is essential for the development of reliable and robust kinetic models. Molecular reconstruction of petroleum fractions comprises the group of methods that allow to create mixtures of molecules from some analytical data. Using only common R&D analytical data, the statistical reconstruction technique calculates the chemical composition of diesel cuts in terms of 28 chemical families by carbon number groups (C_1–C_{30}). The input data for the reconstruction method are the elementary analyses (sulfur, nitrogen), density, simulated distillation (SimDist) and mass spectrometry [8,9]. The properties of each pseudo-compound can be obtained by direct inspection or calculated by group contribution methods. Furthermore, mixing rules are used to determine the mixture properties from the composition and the pseudo-compound properties. This statistical reconstruction method was applied to accurately "reconstruct" different gas oils such as light cycle oils (LCO), straight run gas oils (SR) and coker gas oils (CGO).

Using the detailed chemical composition of the feedstocks and effluents, a kinetic model for gas oil hydrotreatment was

developed. A Langmuir–Hinshelwood representation was adopted for this kinetic model implementing the current knowledge of reaction schemes for hydrodearomatization (HDA) and hydrodenitrogenation (HDN) in the model. Concerning the HDS reactions, a detailed study of the different reactivities of alkylated dibenzothiophenes was carried out and three different families of refractory compounds were distinguished in order to improve the prediction accuracy of the residual sulfur. Since this kinetic model is based on a detailed characterization of hydrocarbons by family and boiling point, it presents many advantages in comparison to classic "lumped" models. Some advantages among others are: (1) the vapor–liquid distribution and composition obtained by flash calculation is more accurate, (2) the mass and molar balances are verified directly with the stoichiometry of the reactions, (3) cracking reactions can easily be incorporated, (4) it is possible to directly calculate some macroscopic properties of the hydrotreated products such as hydrogen content, aromatic carbon or even simulated distillation. The parameters of the model were fitted on different experiments carried out on pilot plant facilities with actual gas oil feedstocks using industrial hydrotreatment operating conditions. An accurate prediction of the product composition has been obtained for the entire set of experimental data. This kinetic model is therefore used to determine the operating conditions of hydrotreating units necessary to achieve the current specifications of commercial fuels.

Refining targets do not only concern productivity and selectivity: the safe operation of industrial units is also a high-priority topic. Indeed, hydrotreating processes consist of hydrogenation and hydrogenolysis reactions that are highly exothermic. For the hydrotreatment of middle distillates, the reaction heat release is mainly due to the hydrogenation of aromatics, olefins and HDS reactions. Therefore, from the thermal control point of view, hydrotreating of straight run gas oils is much more straightforward compared to hydrotreating light cycle oils. Indeed, LCOs contain high amounts of unsaturated compounds (generally more than 70 wt.%) and their hydrotreatment represents a runaway risk. Similarly, CGOs contain large amounts of reactive olefins, whose hydrogenation also results in a significant heat release. Therefore, the incorporation of higher amounts of these feeds must be ensured by a thermal stability analysis. It is well known that the stationary stability characterized by the van Heerden criterion [10] must be satisfied. However, this is not sufficient to ensure the actual reactor stability. Only a dynamic analysis can provide an accurate answer concerning the safe operation of the reactor. For this purpose, a 1D dynamic model that accurately represents the reactive system (gas–liquid–solid) was developed and validated with experimental pilot plant data. The model takes into account a detailed description of the reactive system and the configuration of an existing IFP pilot plant: the three phases (gas–liquid–solid), the HDT kinetics, the flow characterization in the gas and liquid phases, the heating devices and the control system. An experiment was carried out in the pilot plant to collect dynamic data for the model validation. The model was the basis to perform the thermal stability analysis according to stationary and dynamic criteria. The reactor behavior is accurately predicted with this stability analysis method.

2. Statistical reconstruction of gas oil fractions

The use of kinetic models in refining is very often limited by the molecular complexity of the petroleum fractions. Indeed, oil mixtures are composed of thousands of different chemical compounds according to their distillation cut points (gasoline, kerosene, gas oil, vacuum distillates, atmospheric residues and more). For this reason, it is very difficult, or even impossible, to measure the abundance of all the molecular species present in petroleum cuts. To get over this analytical limitation, numerous efforts have been made to develop molecular reconstruction methods in order to characterize the petroleum fractions by mixtures of chemical compounds derived from average and partial analyses [11–22]. In the particular case of gas oil characterization, a new method developed at IFP and based on statistical distributions for the length of the alkyl side chains is proposed in this article.

Table 1
Listing of the selected chemical families reconstructed and used in the kinetic model.

Index	Chemical family	Reactivity group
1	Paraffins	SAT
2	Cyclohexanes	SAT
3	Perhydronaphthalenes	SAT
4	Perhydroanthracenes	SAT
5	Benzenes	MONO
6	Tetralins	MONO
7	Dinaphthenobenzenes	MONO
8	Naphthalenes	DI2
9	Tetrahydroanthracenes	DI2
10	Dihydroanthracenes	DI1
11	Anthracenes	TRI
12	Pyrenes	TRI
13	Bicyclohexyls	SAT
14	Cyclohexylbenzenes	MONO
15	Biphenyls	DI1
16	Sulfides/thiols	SULF
17	Thiophenes	SULF
18	Benzothiophenes	BT
19	Alkyldibenzothiophenes	DBT1
20	4-Alkyldibenzothiophenes	DBT2
21	4,6-Alkyldibenzothiophenes	DBT3
22	Anilines	NBAS
23	Pyridines	NBAS
24	Quinolines	NBAS
25	Acridines	NBAS
26	Pyrroles	PYRR
27	Indoles	IND
28	Carbazoles	CARB

2.1. Characterization of gas oils in the form of molar matrices of pseudo-compounds

2.1.1. Description of the matrix

The matrix of pseudo-compounds is described by using 28 different chemical families: 15 hydrocarbon families, 6 sulfur families and 7 nitrogen families. Table 1 indicates in the 'Index' and 'Chemical Family' columns the detailed hydrocarbon and heteroatomic families taken into account by the statistical reconstruction method. The choice of the families is mainly based on the available information obtained from mass spectrometry [8,9] and sulfur and nitrogen speciations. The following hypotheses were assumed:

- alkyl chains and paraffins are considered to be linear,
- all the naphtheno-aromatic cores are described by using cycles with 6 carbon atoms, excluding cycles with 5-carbon atoms cycles as cyclopentane,
- no olefinic families are included,
- the alkyl-dibenzothiophenes family is divided into three subfamilies to take into account their activity differences (see Section 3).

For each of these families, a distribution by carbon number (from 1 to 30) is considered, resulting in a final matrix of 597 pseudo-compounds (all isomers included). The latter number is obtained after eliminating impossible pseudo-compounds such as an alkyl aromatic with four carbon atoms in total for example. In this way, each pseudo-compound of the matrix is characterized by

a chemical family and a carbon atom number, which correspond to both dimensions of the matrix. This type of description has already been used, for example, for the analytical development of gas chromatography in combination with a mass spectrometer (GC–MS) [23] or for representing gas oil fractions [15].

2.1.2. Properties of the pseudo-compounds in the matrix

Once the matrix is defined, it is necessary to calculate the properties of the pseudo-compounds in order to subsequently calculate the properties of the mixture. For the present purpose, the properties considered are the following:

- chemical formula (carbon, hydrogen, sulfur and nitrogen),
- molecular weight,
- aromatic, naphthenic and paraffinic carbon content,
- normal boiling point,
- molar volume at 15 °C and 20 °C.

The chemical formula, the molecular weight and the aromatic, naphthenic and paraffinic carbon contents are calculated directly from the structure of the pseudo-compounds. The normal boiling point and the molar volume are determined from modified group contribution methods [20]. Concerning the normal boiling point, the method used consists in taking the normal boiling point of the head of the homologous family which is obtained from the literature and then adding a contribution for each aliphatic carbon in the alkyl chains:

$$\exp\left(\frac{T_b}{307.63}\right) = \exp\left(\frac{T_{b,head}}{307.63}\right) + 0.31012 nC_{alph} \quad (1)$$

where T_b is the pseudo-compound boiling point, $T_{b,head}$ is the boiling point of the head of the corresponding family and nC_{alph} is the number of aliphatic carbon atoms in the alkyl chains. For the molar volume (at 20 °C) a similar approach is applied as indicated in Eq. (2):

$$V_m^{20} = V_{m,head}^{20} + 16.38 nC_{alph} \quad (2)$$

where V_m^{20} is the molar volume of the pseudo-compound at 20 °C and $V_{m,head}^{20}$ is the molar volume at 20 °C of the head of the corresponding family. To calculate the molar volume at 15 °C, a simple temperature correction is carried out:

$$V_m^{15} = 1.00352 V_m^{20} - 0.2600 \quad (3)$$

It is also possible to calculate other properties such as the critical properties, the Rackett's compressibility factor or the acentric factor. This information is very useful for example as input data for reliable flash calculations.

2.2. Determination of the mixture properties

Petroleum mixtures, as the majority of complex chemical mixtures, are far from having an ideal thermodynamic behavior. While some mixture properties can easily be deduced from the pseudo-compounds matrix by mass balance (elementary analysis, average molecular weight, etc.), this is not the case for more complex properties such as the average density or the distillation curve. For these last ones, mixing rules or simplifying assumptions have to be introduced. In the case of the distillation curve, the hypothesis consists in assuming a true boiling point distillation (TBP). This means that the pseudo-compounds are ideally separated by their increasing individual normal boiling points. For the average density, the mixture is assumed to be ideal with no excess molar volume calculation. However, this assumption creates a bias which can be evaluated after reconstruction of several gas oils and comparison with experimental average densities. After the evaluation of the bias, the average density of a gas oil mixture was finally corrected by means of the following equation:

$$d = \frac{MW}{0.9404 \sum_{i=1}^{N_{comp}} x_i V_{m,i}^{15} + 12.8} \quad (4)$$

where d is the average density of the mixture at 15 °C (g/cm^3), MW is the average molecular weight of the mixture (g/mol), $V_{m,i}^{15}$ is the molar volume of the pseudo-compound i at 15 °C (cm^3/mol) and x_i is the molar fraction of the pseudo-compound i (dimensionless).

On the basis of the mixing rules developed in this work, it is possible to link a molar fractions matrix of pseudo-compounds to its mixture properties. The next step is now to determine the molar fractions of different gas oils as a function of their analytical characteristics. This complex work is managed by the statistical reconstruction method described below.

2.3. The statistical reconstruction method

2.3.1. Theoretical aspects

The principle of the statistical reconstruction is based on two hypotheses:

- the length of the alkyl side chains (considered as linear) that are connected to naphtheno-aromatic cores follows a statistical distribution. The same distribution is applied to all side chains and was chosen to be a gamma distribution whose standard representation is shown in Fig. 1,
- for the chemical families without a polycyclic core (paraffins and sulfides/thiols), a different standard gamma-type distribution (cf. Fig. 1) is used for the length of the alkyl chains.

The choice of the gamma functions is based on experimental carbon number distribution obtained from GC–MS analyses [23] of various gas oils. With these general assumptions, it is possible to estimate, for each chemical family, a normalized (to 1) molar carbon number distribution of the pseudo-compounds within their chemical family. These normalized distributions are then used to calculate the average molecular weight of each chemical family. The analytical data, i.e., Fitzgerald mass spectrometry, sulfur speciation and nitrogen speciation, are combined to determine the mass and molar fractions of the 28 chemical families. Finally, combined with the normalized molar distributions of each chemical family, it is possible to calculate the molar composition of the pseudo-compounds by redistributing by carbon number and to establish in this way the molar fractions of the 597 pseudo-compounds of the matrix.

2.3.2. Standard molar distributions for chemical families with a polycyclic core

Establishing a normalized molar distribution for each chemical family with a polycyclic core requires three important data:

- the maximum number of alkyl chains, N_{chains}, that can be added to the representative core of the chemical family. To calculate this value, it has been assumed that only the aromatic CH and the naphthenic CH_2 carbon atoms can accept one side chain per carbon,
- the standard distribution of the side chains (Fig. 1),
- the maximum length of a side chain, noted L. L can be any positive real number since the reconstruction method is a statistical method.

By default, the smallest pseudo-compound in a chemical family consists of a naphtheno-aromatic core with no side chains. The

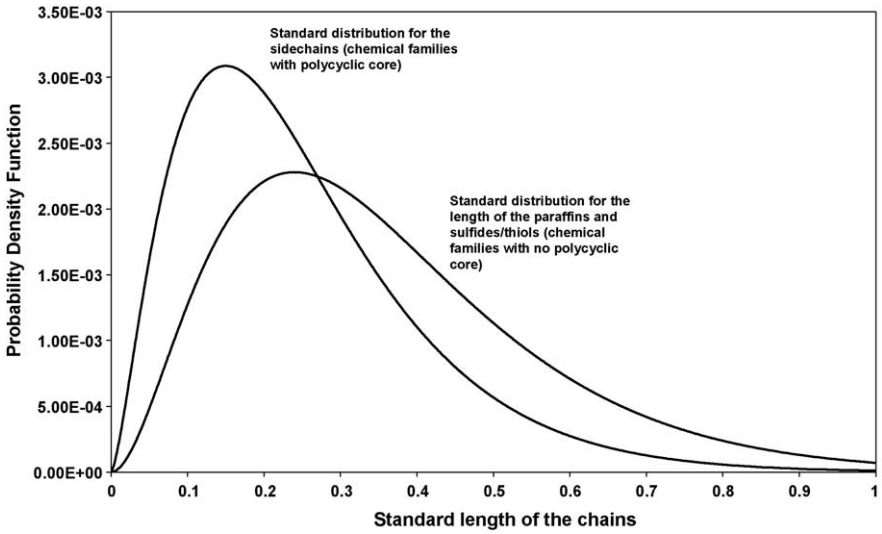

Fig. 1. Standard distribution for the length of the side chains or for the length of the paraffins and sulfides/thiols.

heaviest consists of the same core with N_{chains} side chains with L carbon atoms. All pseudo-compounds within these two limits are then present and their relative content is fixed by the normalized molar distribution.

For example, for the alkyl benzene family, a maximum of six side chains can be added, one per aromatic CH carbon atom. Assuming a maximum side chain length L of 2.0, the smallest pseudo-compound in the alkyl benzene family is the benzene (C_6 alkyl benzene) and the heaviest is an alkyl benzene in C_{18} (6 carbon atoms for the core + 6 side chains × 2.0 carbon atoms per side chain maximum = 18). The standard distribution shown in Fig. 1 can then be homothetically transformed and then discretized in order to obtain the normalized distribution of the alkyl benzene family, between C_6 and C_{18} (Fig. 2).

However, the calculation of a molar fraction distribution for each chemical family in the matrix is not complete because the distillation cut points have not yet been taken into account. For example, if the gas oil cut to be reconstructed is a 160–400 °C fraction, pseudo-compounds whose normal boiling point is below 160 °C or above 400 °C cannot be present in such a cut. Therefore, they have to be removed from the distribution. Hence, to take into account the boiling point range of the gas oil cut, a separation efficiency factor was applied according to the following rules:

- if the pseudo-compound has a normal boiling point outside the boiling point range of the gas oil, the separation efficiency factor η is fixed to 0,
- if the pseudo-compound has a normal boiling point between the 10 wt.% and the 90 wt.% boiling point, the molar fraction is retained with a separation efficiency factor η of 100%,
- if the pseudo-compound has a normal boiling point between the initial boiling point (IBP) and the 10 wt.% boiling point (or between the 90 wt.% boiling point and the final boiling point (FBP)), the molar fraction is modified using a separation efficiency factor η that has a linear behavior between these limits.

Fig. 3 summarizes this approach. With standard distribution of the alkyl benzene family, and assuming that the gas oil fraction to be reconstructed is a 160–400 °C cut, the only alkyl benzenes which can be present in this fraction are C_9 to C_{24} alkyl benzenes. Hence, the distribution shown in Fig. 2 has to be modified to take

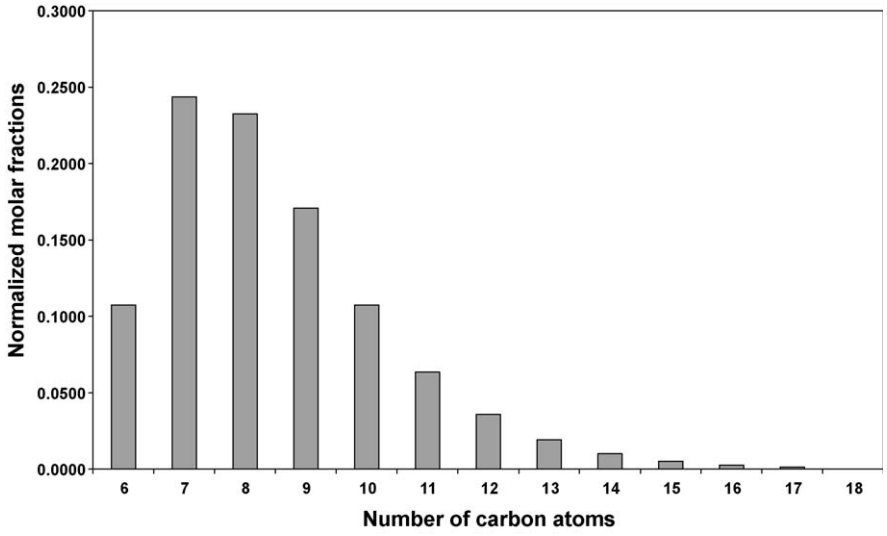

Fig. 2. Example of a discrete distribution for the family of alkyl benzenes with L = 2.0.

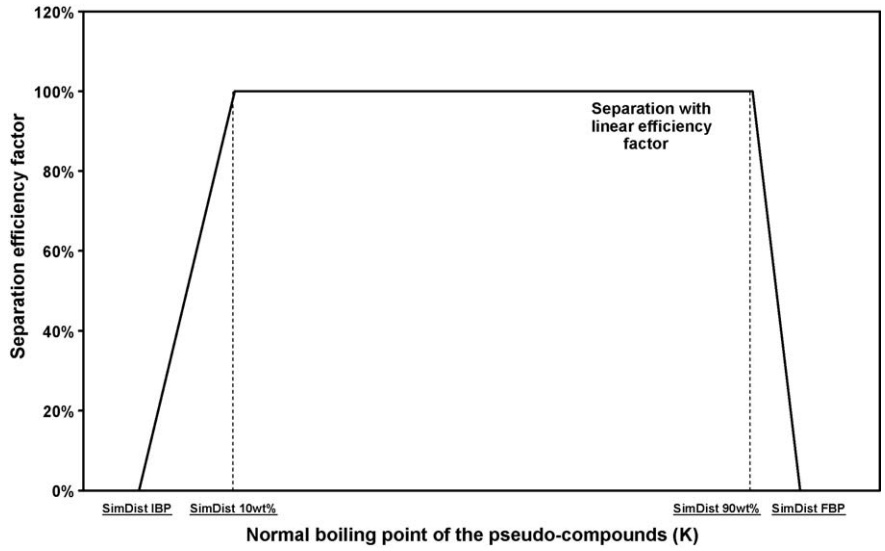

Fig. 3. Method for pseudo-compounds separation in function of the simulated distillation. Separation with a linear efficiency factor.

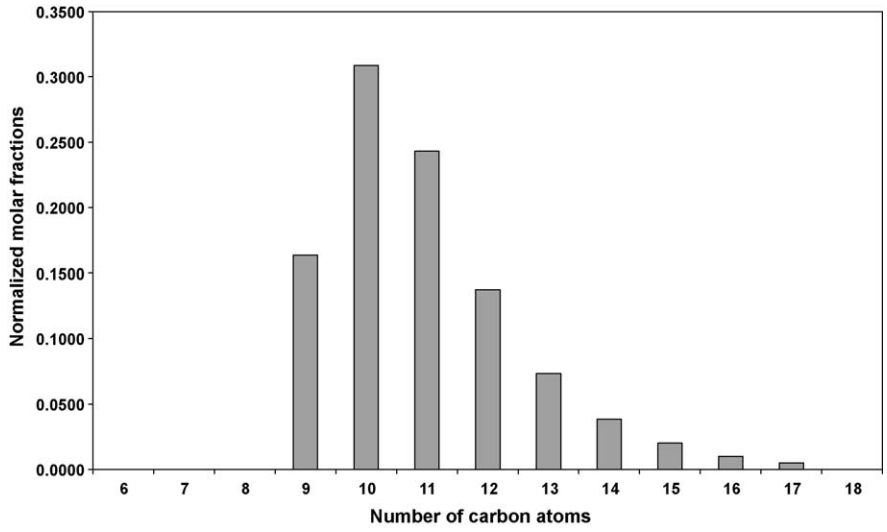

Fig. 4. Example of a discrete distribution for the family of alkyl benzenes with $L = 2.0$ when the distillation cut is 160–400 °C.

this additional constraint into account. Fig. 4 shows the new molar distribution of the alkyl benzene family after cut point correction and renormalization. As shown, C_6, C_7 and C_8 alkyl benzenes are removed, while the abundance C_9 alkyl benzenes are significantly reduced by means of the separation efficiency factor.

2.3.3. Standard molar distributions of paraffins and sulfides/thiols

With chemical families such as the paraffins and the sulfides/thiols, there is no naphtheno-aromatic core and the assumptions regarding the distribution of the side chains can no longer be used. A similar method is followed using the distillation cut points in order to determine the total number of carbon atoms of the smallest and the largest pseudo-compound of the family. A standard distribution is also used (Fig. 1) which is again homothetically transformed between these two extreme pseudo-compounds. The remainder of the procedure is identical.

2.3.4. Determination of the overall content of the chemical families

Once the renormalized distributions of each of the chemical families have been determined, they have to be quantified globally. The reconstruction requires three chemical analyses: Fitzgerald mass spectrometry (MS) [8,9], sulfur speciation [1] and nitrogen speciation. The weight fractions of hydrocarbon families are obtained by mass spectrometry while the sulfur and nitrogen analyses give the mass fractions of the sulfur and nitrogen families in weight ppm of sulfur or nitrogen respectively. To determine the overall mass fractions of the chemical families, one needs to combine these three analyses. However, as they are expressed on a different basis, the average molecular weight of each family is needed. This is done using the previously calculated molar distributions.

It must be pointed out that these three analyses are independent and not consistent between each other. Indeed, each one has its intrinsic analytical uncertainties. In addition, the Fitzgerald mass spectrometry analysis applied in this work [8,9] does not quantify nitrogen compounds. Hence, they have to be renormalized so that the sum of the mass fractions of all the chemical families is equal to 1. Because the uncertainty of the mass spectrometry is the largest of the three analyses, the renormalization is only applied to the hydrocarbon families. To convert the

mass fractions into molar fractions, each of the mass fractions of the chemical families is divided by their average molecular weight and then renormalized to 1.

Concerning the hydrocarbons mass spectrometry analysis, it must be stressed that the method quantifies four saturated hydrocarbons families and eight aromatic hydrocarbons families. The saturated hydrocarbons correspond to the next condensed formulas: C_nH_{2n+2}, C_nH_{2n}, C_nH_{2n-2} and C_nH_{2n-4} and the aromatic hydrocarbons to the following formulas: C_nH_{2n-6}, C_nH_{2n-8}, C_nH_{2n-10}, C_nH_{2n-12}, C_nH_{2n-14}, C_nH_{2n-16}, C_nH_{2n-18}, and C_nH_{2n-20+}. 20+. In some cases, the condensed formula may correspond to different chemical structures. For example C_nH_{2n-14} can correspond to acenaphthenes, biphenyls, tetrahydroanthracenes and tetrahydrophenanthrenes. The Fitzgerald mass spectrometry method is not able to quantify separately different chemical families having the same condensed formula, hence only the content of C_nH_{2n-14} family can be determined corresponding to the addition of all these families. For the statistical reconstruction purposes, to fit the mass spectrometry analysis, the contents of bycyclohexyls, cyclohexylbenzenes and byphenyls in the gas oil feeds were considered to be equal to zero. The contents of the other families in the matrix structure are obtained from the mass spectrometry analysis according to their corresponding condensed formulas. Then, for the C_nH_{2n-14} family cited before, the corresponding family in the matrix structure is the tetrahydroanthracenes family.

2.3.5. Determination of the molar fractions matrix

This final step consists in calculating the molar fraction of each individual pseudo-compound from the molar fraction of its chemical family and its molar distribution by carbon number. In this way, the gas oil cut is characterized by a molar fractions matrix from which the properties of the mixture can be determined. By construction, the quantities of the sulfur and nitrogen families in the matrix are strictly equal to the quantities obtained by the sulfur speciation and the nitrogen speciation. The mass spectrometry of the matrix differs very slightly from the one of the gas oil cut due to the renormalization. The average molecular weight and the distillation curve of the reconstructed mixture strongly depend on the value chosen for the maximum length of the side chains L and of the chosen IBP and FBP. These mixture properties may therefore be completely off, and need to be adjusted by modifying the value of the maximum length of the side chains L, which becomes a parameter to be optimized.

2.3.6. Optimization of the model parameters

Mass spectrometry, sulfur speciation and nitrogen speciation provide chemical information with respect to the gas oils; this is used to reconstruct the "chemical" dimension of the matrix. However, it is also necessary to have some information concerning the second dimension of the matrix, i.e., on the carbon number distribution. Simulated distillation (SimDist) seems to be the most appropriate analysis for this purpose. On the basis of correlations, SimDist can also be used to estimate the average molecular weight of the gas oil cut. Moreover, as stated before, the initial and the final boiling points (IBP and FBP respectively) are essential to establish the molar distributions.

However, it must be noted that these two cut points, the initial and final boiling points, have very large analytical uncertainties. That is why it was decided to use the average molecular weight, and the 10 wt.% and 90 wt.% points of the simulated distillation as analytical targets during the reconstruction of the second dimension. The parameters to be optimized are therefore the following:

- L: the maximum length of the side chains (which greatly influences the average molecular weight of the mixture),
- IBP: the initial point of the simulated distillation,
- FBP: the final point of the simulated distillation.

As indicated in Fig. 5, at each iteration, the pseudo-compounds matrix is recalculated together with its mixture properties. The mass spectrometry, sulfur speciation and nitrogen speciation are always very close to the analytical data by construction. Distillation data (SimDist 10 wt.% and 90 wt.%) and the molecular weight converge towards their experimental values when the parameters of the model are modified. Upon convergence, the resulting pseudo-compounds matrix has properties that are very close to those given by the mass spectrometry, the sulfur speciation, the nitrogen speciation and the simulated distillation. This final pseudo-compounds matrix is then taken as representative of the gas oil to be reconstructed.

2.4. Application to the reconstruction of gas oils

The statistical reconstruction method was applied to reconstruct a diversity of gas oils. This paragraph details the results of a straight run (SR) gas oil. Density, SimDist, mass spectrometry, sulfur speciation and nitrogen speciation of this SR gas oil were used as input data. The analytical data available for this gas oil is given in Table 2. The average molecular weight of this gas oil was estimated according to API correlations from SimDist and density data, and was found to be 242.5 g/mol. The optimization of L, IBP and FBP was performed in order to fit a pseudo-compound mixture with the following properties:

- average molecular weight: 242.5 ± 5.0 g/mol,
- 10 wt.% SimDist point: 245 ± 5.0 °C,
- 90 wt.% SimDist point: 376 ± 5.0 °C.

The reconstruction results after optimization are given in Table 2. The reconstructed matrix has a molecular weight of 240.5 g/mol. As indicated in Table 2, a 10 wt.% SimDist point of 250 °C and a 90 wt.% SimDist point of 378 °C are obtained, which is within the required uncertainty. With this matrix, the maximum length of the alkyl chains is 4.0, the SimDist initial boiling point is 215.6 °C and the SimDist final boiling point is 447.4 °C. It should be also stressed that there is an excellent agreement between the experimental and calculated mass spectrometry analysis. Thus, accordingly to these results, the representation of this gas oil by the pseudo-compounds matrix is certainly close to its actual detailed composition by chemical family and by carbon number.

The reconstruction method has been extended to any type of diesel fractions. Hence, a large variety of gas oils has been reconstructed. Among these gas oils, there are various SR gas oil, light cycle oils, coker gas oils as well as several mixtures:

- 8 straight run gas oils (Middle East, West African, Maya, etc.),
- 7 light cycle oils,
- 2 coker gas oils,
- 7 mixtures (SR + LCO, SR + coker, SR + LCO + coker).

After reconstruction, it was possible to predict the density, the hydrogen content and aromatic carbon content of the associated matrices which are not analyses used for the reconstruction. The parity plots in Figs. 6–8 illustrate the comparison between analytical data and the calculated properties. Excellent results were obtained on the whole set of gas oils, also confirming that gas oil fractions are accurately represented by means of this novel statistical reconstruction approach.

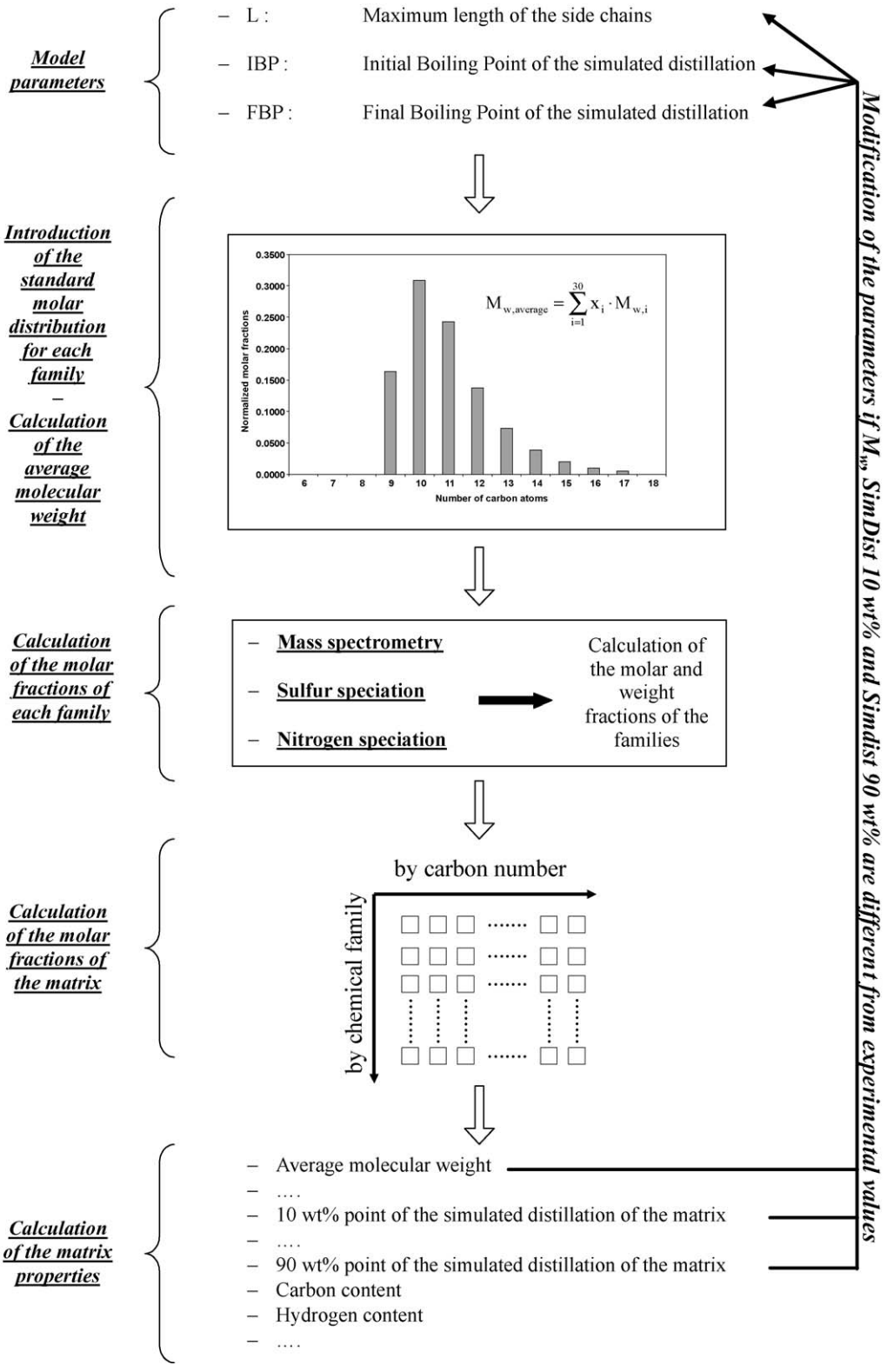

Fig. 5. Diagram of the statistical reconstruction of gas oils.

2.5. Olefins handling

It must be stressed that diesel fractions such as light cycle oils and coker gas oils have a high content of olefins. The Bromine Number method (ASTM D1159) is used to estimate the percentage of olefins in petroleum distillates. Nevertheless, there is no analytical method that allows to quantify and to distinguish the different types of chemical structures where an olefinic bond is present (paraffinic, naphthenic, chain linked to a naphtheno-aromatic core, etc.). The reference analysis used in this work to quantify the major hydrocarbon families is the Fitzgerald mass spectrometry [8,9]. Since this method does not either quantify olefins and there is no other reference method to quantify this family, the statistical reconstruction presented in this work fits

Table 2
SR gas oil analyses and associated pseudo-compounds mixture properties.

Properties	Units	Properties of the calculated matrix	Analytical data
Density	g/cm^3	0.8548	0.8537
Hydrogen content	wt.%	13.32	13.25
Total sulfur content	wt.%	1.35	1.35
Total nitrogen content	wt.%	0.0127	0.0127
Aromatic carbon content	%	13.24	15.0
Simulated distillation (SimDist)			
0 wt.%	°C	216	160
5 wt.%	°C	245	219
10 wt.%	°C	250	245
20 wt.%	°C	269	272
30 wt.%	°C	284	290
40 wt.%	°C	301	304
50 wt.%	°C	315	317
60 wt.%	°C	328	330
70 wt.%	°C	342	344
80 wt.%	°C	360	359
90 wt.%	°C	378	376
95 wt.%	°C	394	386
100 wt.%	°C	447	404
Mass spectrometry chemical families (MS)			
C_nH_{2n+2}	wt.%	40.63	41.9
C_nH_{2n}	wt.%	16.77	17.3
C_nH_{2n-2}	wt.%	8.24	8.5
C_nH_{2n-4}	wt.%	2.04	2.1
C_nH_{2n-6}	wt.%	7.66	7.9
C_nH_{2n-8}	wt.%	3.39	3.5
C_nH_{2n-10}	wt.%	1.36	1.4
C_nH_{2n-12}	wt.%	4.65	4.8
C_nH_{2n-14}	wt.%	1.94	2.0
C_nH_{2n-16}	wt.%	1.26	1.3
C_nH_{2n-18}	wt.%	1.26	1.3
C_nH_{2n-20+}	wt.%	0.00	0.0
Sulfur speciation (GC–SCD)			
Sulfides/mercaptans	wt ppm S	7226	7226
Thiophenes	wt ppm S	0	0
Benzothiophenes	wt ppm S	2081	2081
Dibenzothiophenes	wt ppm S	937	937
4-Dibenzothiophenes	wt ppm S	1821	1821
4,6-Dibenzothiophenes	wt ppm S	1435	1435
Nitrogen speciation (GC–NCD)			
Anilines	wt ppm N	0	0
Pyridines	wt ppm N	0	0
Quinolines	wt ppm N	47	47
Acridines	wt ppm N	0	0
Pyrroles	wt ppm N	0	0
Indoles	wt ppm N	40	40
Carbazoles	wt ppm N	40	40

only the major hydrocarbon families available. For the detailed kinetic model described in Section 3, olefins were considered to be extremely reactive and directly hydrogenated at the reactor inlet. Their content was calculated by the Bromine Number method (ASTM D1159) and their contribution to hydrogen consumption is taken into account in this way.

3. Kinetic modeling of gas oil hydrotreatment

The exhaustive study of hydrotreating reactions is required for the development of reliable kinetic models that allow to determine the most appropriate conditions to attain commercial diesel specifications. Among the physico-chemical properties submitted to legislation, in numerous countries including the European Union (EU), USA and Japan (among others), the maximum total sulfur content has been radically reduced to levels as low as 10 wt ppm. For this reason, the different reactivities of the most refractory sulfur compounds present in middle distillates have been largely studied. The sulfur compounds present in gas oils are a complex mixture of mercaptans, sulfides and thiophenic compounds. It is well known that the alkyl-dibenzothiophenes (DBTs) are the most refractory sulfur compounds in diesel cuts. Literature works, carried out with model molecules, largely report the reactivities of DBTs [24–33]. The reactivity of these compounds considerably decreases when the alkyl substituents are located close to the sulfur atom. Thus, 4,6-dimethyldibenzothiophene (4,6-DMDBT) is a typical refractory sulfur compound. This refractory behavior is explained by the steric hindrance induced by the alkyl chains, which obstruct the carbon–sulfur bond scission. For the DBTs, two hydrodesulfurization pathways have been proposed: the direct hydrogenolysis pathway, followed by the most reactive DBTs, and the hydrogenation pathway. The latter one consists in an initial hydrogenation of one aromatic ring before the carbon–sulfur scission, and is the most preferential pathway for the most refractory DBTs. The inhibitor effect of other chemical families present in industrial feeds on HDS performances has also been studied. Organic nitrogen compounds present in diesels are divided into two types: basic (pyridinic) and non-basic (pyrrolic). Even if these compounds are present gas oils in much lower amounts (about 100–800 wt ppm of total N), HDS performances are significantly affected by their presence [34–40]. Not only is their amount important, but also their type. Basic nitrogen compounds such as acridines have a strong inhibiting effect on HDS, while non-basic nitrogen species such as carbazoles are even more refractory to hydrotreatment than DBTs [34].

Aromatics are also undesirable chemical families in diesel cuts. The diaromatics + (diaromatics + triaromatics + polyaromatics) content is restricted to maximum 11 wt.% in EU commercial diesel fuels. Furthermore, aromatics are detrimental for the cetane number, which is also subject to legislation (CN ASTM D613 $\geq$51 in EU).

As indicated in last paragraphs, extensive works have been reported mainly for model molecules. Kinetic studies using actual gas oil feeds are not frequent. Indeed, the complexity of the feeds as well as the inhibiting effect of the various chemical families renders the study of the entire set of HDT reactions intricate. Some studies with industrial feeds are reported in the literature [41–48]. Steiner et al. [41] presented a pseudo-first-order kinetic study of four individual dibenzothiophenes and the effect of temperature on HDS conversion. Chen et al. [46,47] evaluated the reactivities of 14 alkyl-dibenzothiophenes. A two-route HDS model, comprising a hydrogenation and a hydrogenolysis pathway, was used to fit the experimental data. In a more extensive approach, Chowdhury et al. [43] and Pedernera et al. [44] developed a more detailed model that accounts for HDS, HDA and HDN reactions using a Langmuir representation. In their work, the HDS kinetics is calculated based on information concerning the aromatic sulfur compounds but no indication is reported about the nature of these compounds.

In this work, a lumped kinetic model with a break-down by carbon number was developed. As indicated in Section 2, the detailed composition of gas oils (feeds and products) is calculated via statistical reconstruction. The kinetic model takes into account the overall HDT reactions: hydrodesulfurization, hydrodearomatization and hydrodenitrogenation.

3.1. Experimental

All the HDT experiments were carried out in pilot plant facilities. All feeds are industrial gas oils of different types: straight runs from a large variety of crude oils, light cycle oils, coker gas oils and their mixtures. The HDT operating conditions covered a wide range and were in all cases representative of those practiced in industrial units: temperature from 320 to 360 °C, liquid hourly space velocity (LHSV) from 0.3 to 4 h^{-1} and hydrogen partial

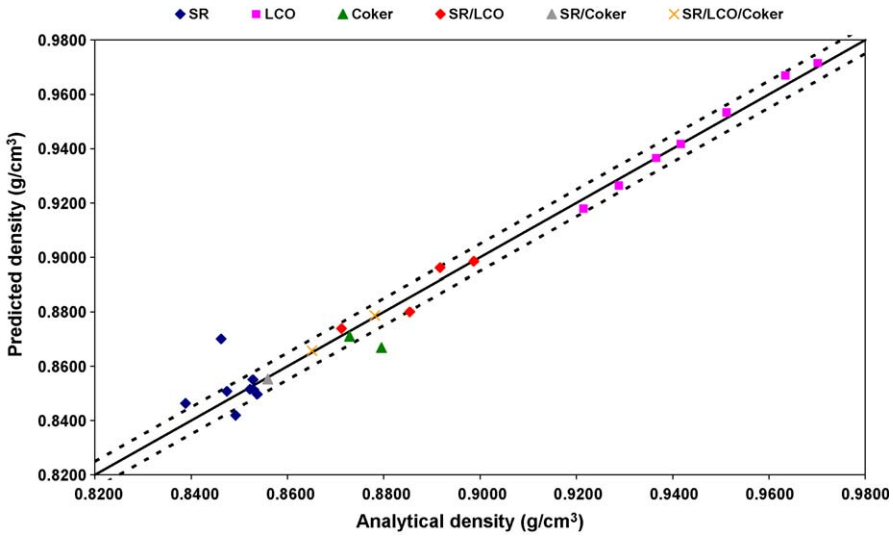

Fig. 6. Parity plot of the prediction of gas oils density by statistical reconstruction. Dotted lines, ±0.005 g/cm^3.

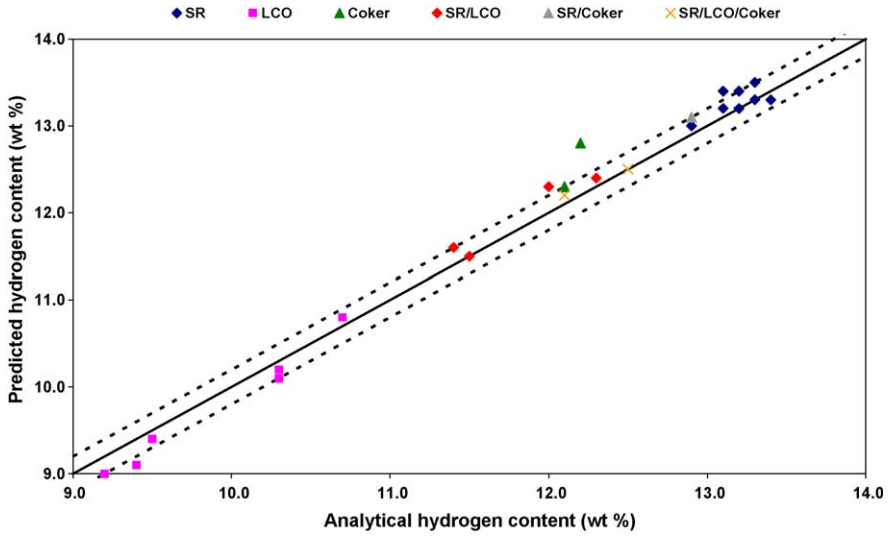

Fig. 7. Parity plot of the prediction of gas oils total hydrogen content by statistical reconstruction. Dotted lines, ±0.2 wt.%.

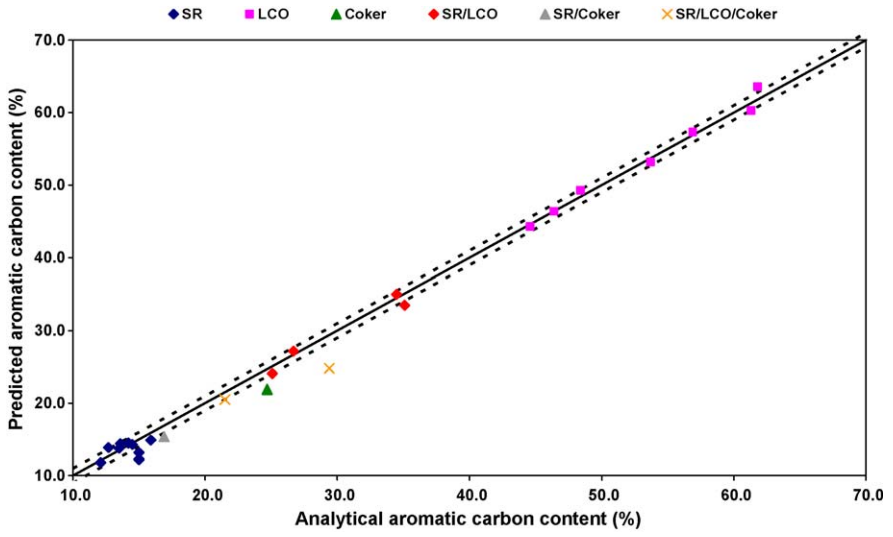

Fig. 8. Parity plot of the prediction of gas oils aromatic carbon content by statistical reconstruction. Dotted lines, ±1%.

pressure from 13 to 100 bar. The catalyst is a commercial in situ sulfided $NiMo/Al_2O_3$. The experimental points are obtained as follows: for a given set of operating conditions, once stable operation is reached (constant properties of the outlet product), a mass balance is performed taking into account the analyses of the feed (gas + gas oil) and the product (on-line gas analysis + hydrotreated product). All feeds and hydrotreated products are characterized according to different analyses. Among others, we can mention the standardized ASTM methods: density (ASTM D4052), sulfur (ASTM D2622, ASTM D5453), nitrogen (ASTM D4629), and simulated distillation (ASTM D2287), as well as other in-house methods: sulfur speciation [1], mass spectrometry [8,9].

3.2. Kinetic model

For the development of the HDT kinetic model, a Langmuir–Hinshelwood representation was adopted in order to take into account the competitive adsorption of the different chemical families on the catalyst active sites. Two types of active sites were considered: a site where hydrogenation reactions are carried out (τ) and a hydrogenolysis site (σ) for the scission of C–X bonds where X is a sulfur or a nitrogen atom.

Hydrogen is considered to be adsorbed in its molecular form. For each reaction, the rate determining step is considered to be one of the steps on the catalytic surface, while the adsorption–desorption steps of all chemical species are considered to be in equilibrium. The reactor was considered to operate in plug-flow mode. Since at HDT operating conditions compounds are present in liquid and vapor phase, a flash calculation was incorporated in the reactor model to represent both phases, which were considered to be at thermodynamic equilibrium (no transport limitations).

3.2.1. Reaction scheme

The global reaction scheme is shown in Fig. 9. Fourteen types of reactions were considered for all the chemical families illustrated (scheme applied by carbon number up to C_{30}). They include aromatics hydrogenation (HDA), hydrodesulfurization (HDS) and hydrodenitrogenation (HDN). All the pseudo-compounds considered in the kinetic model are illustrated and associated to a given type of reactivity as indicated in Fig. 9—TRI: triaromatics; DI1: non-condensed diaromatics; DI2: condensed diaromatics; MONO: monoaromatics; SAT: saturates such as paraffins (n + iso) and naphthenes; DBT1: dibenzothiophenes of highest reactivity; DBT2: dibenzothiophenes of intermediate reactivity; DBT3: the most refractory dibenzothiophenes; BT: benzothiophenes; SULF: other sulfur compounds such as mercaptans, sulfides and thiophenes; NBAS: anilines, pyridines, quinolines, acridines; PYRR: pyrroles; IND: indoles, CARB: carbazoles. Table 1 indicates the connection between chemical family and the reactivity group to which it is assigned in the kinetic model. As indicated in Fig. 9, 14 hydrotreating types of reactions are considered: 4 hydrodearomatization reactions ((1)–(4)), 6 hydrodesulfurization reactions ((5)–(8), (13) and (14)) and 4 hydrodenitrogenation reactions ((9)–(12)). The reversibility of aromatics hydrogenation was taken into account for reactions (1)–(3). The arrows in dotted lines correspond to very fast reactions which are always 100% conversion, even at the least severe HDT operating conditions. Hence, for modeling purposes, these reactions were considered to be instantaneously carried out at the reactor inlet.

Since the reaction scheme is applied to the 597 pseudo-compounds obtained by statistical reconstruction, this modeling approach gives rise to several advantages. First of all, if we consider only a global characterization of the feed (such as the mass spectrometry by chemical family), the differences of boiling points of the molecules in a lump cause differences of molecular weights inside a lump. In this case, the various compounds are not explicitly taken into account and this may lead to a material balance problem. In other words, in a lumped model, there is no direct relationship between the stoichiometry of the reactions and the average molecular weight of the lumps, so, to maintain the material balance, the molecular weight of the lumps must vary all along the reactor. The model proposed in this work automatically solves this problem since the first dimension of the gas oil reconstruction matrix contains the information concerning the

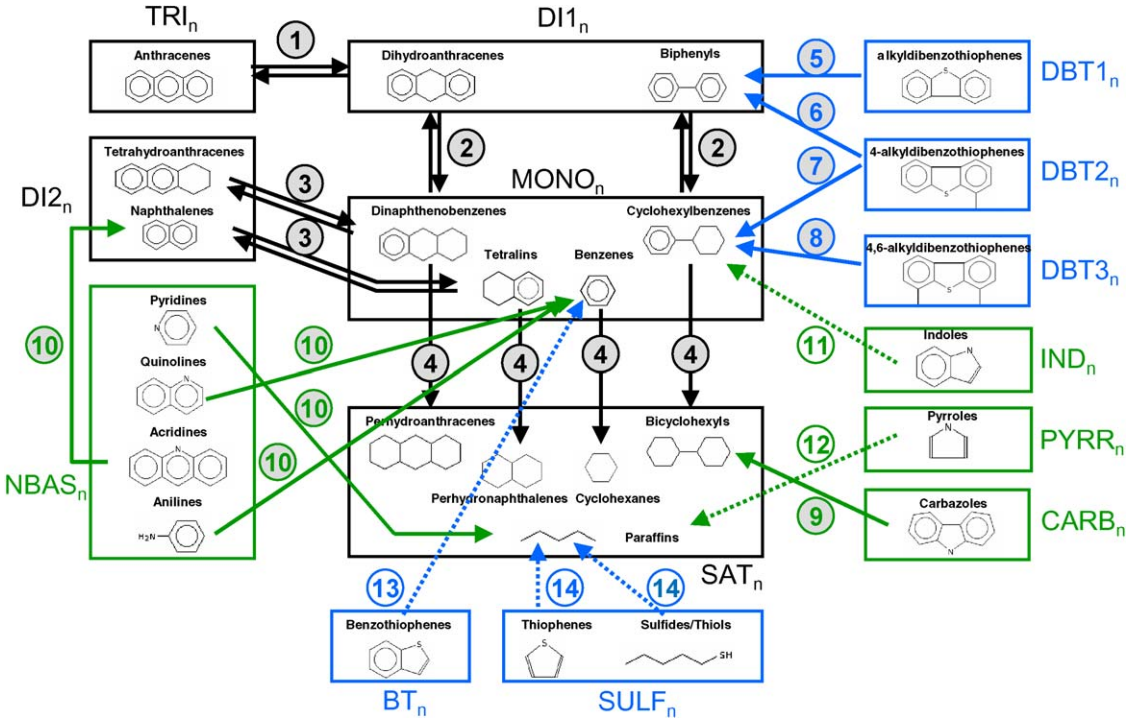

Fig. 9. Reaction scheme of gas oils hydrotreating for each pseudo-compound (28 chemical families by *n* carbon number up to C_{30}).

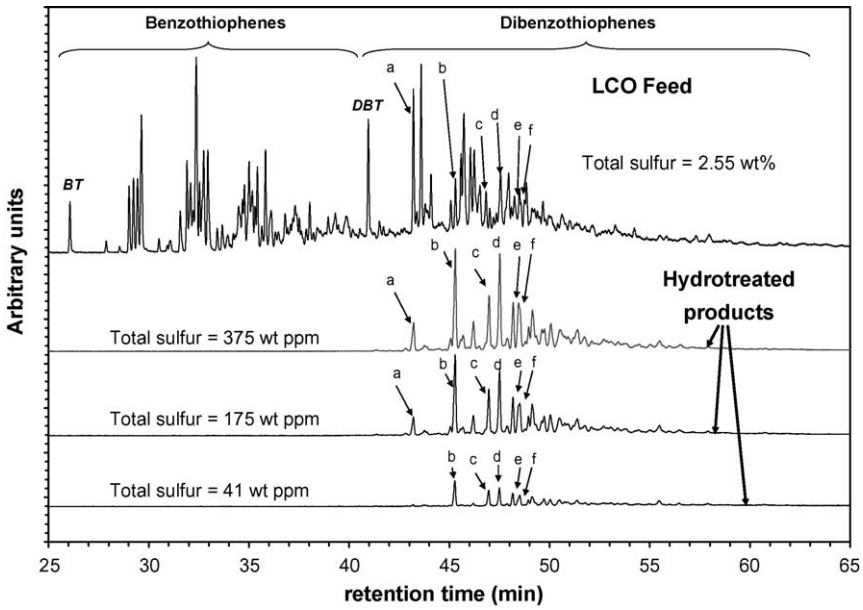

Fig. 10. GC–SCD sulfur speciation profiles of a LCO feed and of three different hydrotreated products. Refractory dibenzothiophenes marked: (a) 4-MDBT, (b) 4,6-DMDBT, (c) 4-M,6-EDBT, (d) 2,4,6-TMDBT, (e) 1,4,6-TMDBT, and (f) 4,6-DEDBT + 3,4,6-TMDBT.

chemical structure (general chemical formula ex. C_nH_{2n-18}) and the second dimension allows to determine the actual condensed formula (ex. for $n = 18$: $C_{18}H_{18}$). Hence, it is possible to solve the reaction scheme by carbon number respecting the overall material balance, as well as the elemental balances (C, H, S, N). Another interesting advantage of disposing of the gas oil reconstruction matrix and the pseudo-compounds properties (molar fractions, critical temperatures, acentric factors) is that the determination of vapor–liquid distributions at HDT conditions is straightforward. Finally, at the outlet of the HDT simulator, it is also possible to accurately estimate various properties of the hydrotreated product such as density, aromatic carbon content or cetane number.

3.2.2. Hydrodesulfurization reactions

Since deep hydrodesulfurization is an essential issue for refiners, a particular effort was made to correctly predict ultra-low sulfur diesel (ULSD). The feeds and hydrotreated products were all analyzed by sulfur speciation (gas chromatography with a sulfur chemiluminescence detector). As mentioned before, a variety of sulfur families is present in gas oils: mercaptans (R–S–H), sulfides (R–S–R′), disulfides (R–S–S–R′) and aromatic sulfur compounds such as benzothiophenes (BTs) and dibenzothiophenes (DBTs). In the range of the tested operating conditions, only dibenzothiophenes are still present in hydrotreated products. Therefore, the other sulfur families were considered to be converted at the reactor inlet into hydrogen sulfide and the corresponding hydrocarbon(s). The sulfur speciation analyses allow to get access to more detailed information on the reactivity of individual DBTs. Fig. 10 illustrates the sulfur speciation chromatograms of a LCO feed with a total sulfur content of 2.55 wt.%. Three hydrotreated products at different sulfur levels are also shown. As can be noticed, the compounds that remain at low sulfur level are mainly those having two alkyl substituents in 4 and 6 positions. First-order reaction rates of individual alkyl-dibenzothiophenes were also calculated and three groups of reactivity were identified [49]. Hence, all alkyl-dibenzothiophenes were classified according to three different reactivities referred to as DBT1, DBT2 and DBT3, as illustrated in Fig. 11. The most reactive alkyl-dibenzothiophenes are those included in the DBT1 reactivity type. As indicated, the dibenzothiophene molecule (DBT) is included in this reactivity type. A second class of alkyl-dibenzothiophenes having an intermediate reactivity (DBT2) was defined. This category of alkyl-dibenzothiophenes contains molecules having a reactivity close to that of 4-methyldibenzothiophene (4-MDBT): i.e., to a DBT having one methyl substituent in the closest position to the sulfur atom. Finally, last reactivity class DBT3 comprises the most refractory alkyl-dibenzothiophenes. This class contains the 4,6-dimethyldibenzothiophene (4,6-DMDBT) which has two methyl substituents in the nearest positions to the sulfur atom and which is known as one of the most refractory sulfur compounds in diesel cuts. As indicated before, there are two HDS routes: the direct desulfurization route followed by the most reactive DBTs and the hydrogenation pathway that consists of initial hydrogenation of one aromatic ring with subsequent carbon–sulfur scission. The pseudo-compounds having a reactivity corresponding to the DBT1 class were considered to follow only the direct HDS route. The pseudo-compounds having a reactivity corresponding to the DBT3 type

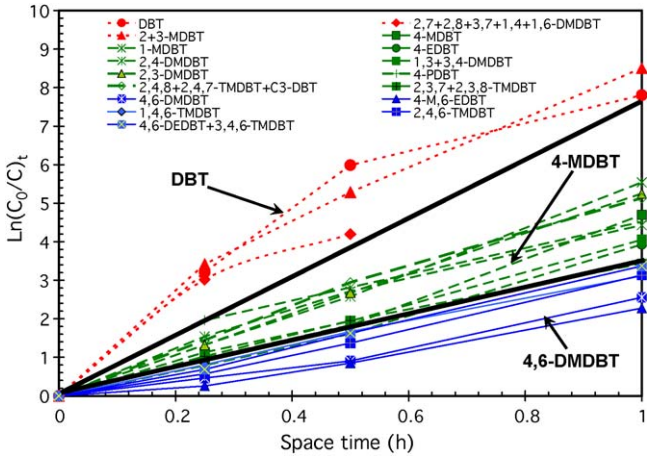

Fig. 11. First-order kinetics plots for different alkyl-dibenzothiophenes.

were assumed to follow preferentially the hydrogenation pathway, and pseudo-compounds having an intermediate reactivity (DBT2) were allowed to follow both pathways. For reactions (5) and (6), the rate determining step was considered to be the C–S scission. For reactions (7) and (8), it was considered that the rate determining step was the first hydrogenation of an aromatic cycle. Based on these hypotheses, the hydrodesulfurization reaction rates for each pseudo-compound (family and carbon number) belonging to a given reactivity class are

$$r_{Alkyldibenzothiophenes,n} = (-k_{5_n} C_{H_2} C_{Alkyldibenzothiophenes,n})\theta_\sigma^2 \quad (5)$$

$$r_{4\text{-}Alkyldibenzothiophenes,n} = (k_{6_n} C_{H_2} C_{4\text{-}Alkyldibenzothiophenes,n})\theta_\sigma^2 + (k_{7_n} C_{H_2} C_{4\text{-}Alkyldibenzothiophenes,n})\theta_\tau^2 \quad (6)$$

$$r_{4,6\text{-}Alkyldibenzothiophenes} = (k_{8_n} C_{H_2} C_{4,6\text{-}Alkyldibenzothiophenes})\theta_\tau^2 \quad (7)$$

where θ_σ and θ_τ are respectively the fraction of free hydrogenolysis and free hydrogenation sites. The reaction rate constants have a subscript n that denotes the dependence of the rate constant on the carbon number.

3.2.3. Aromatics hydrogenation reactions

For the hydrodearomatization reactions (HDA), the pseudo-compounds illustrated in the reaction network (Fig. 9) are hydrogenated according to reactions (1)–(4). Each pseudo-compound has a reactivity type in the HDA reaction scheme. Hence, pseudo-compounds may behave as one of the four types of reactivity indicated in Fig. 9: one type of triaromatics (TRI), two types of diaromatics reactivity (DI1 and DI2) and one type of monoaromatics reactivity (MONO).

Concerning triaromatics hydrogenation, two pathways are possible: hydrogenation of the central aromatic ring or of an external aromatic ring. If both reaction pathways are considered in the reaction scheme, triaromatics are transformed into monoaromatics *via* both pathways. In this case, the kinetic parameters are strongly correlated, however. Literature works [50,51] have reported that the addition of hydrogen in the 9,10 positions of the triaromatic compound to produce a non-condensed diaromatic (DI1 reactivity type) is faster than the hydrogenation of the external ring (to produce a condensed diaromatic). Hence, the triaromatics hydrogenation of the central cycle was preferred and the pathway that hydrogenates the triaromatics such as anthracenes into dihydroanthracenes was retained as indicated in Eq. (8).

$$r_{Anthracenes,n} = (-k_{1_n} C_{Anthracenes,n} C_{H_2} + k_{-1_n} C_{Dihydroanthracenes,n})\theta_\tau^2 \quad (8)$$

Regarding diaromatics hydrogenation, two types of behaviors were distinguished since their reactivity strongly depends on the neighboring position of both rings [50–53]. Non-fused aromatic rings have a reactivity close to that of monoaromatic molecules, while the condensed diaromatics will have a much higher reactivity. Moreau et al. [50] reported relative rate constants for model molecules taking the benzene hydrogenation (relative rate constant = 1) as reference. In this way, the relative rate constants for hydrogenation of biphenyl, fluorene and 9,10-dihydrophenanthrene are 1.5, 2 and 2 respectively, while naphthalene is hydrogenated 10 times faster than benzene. For this reason, dihydroanthracenes were associated to a DI1 reactivity category as well as biphenyls, whereas aromatics having two condensed rings such as tetrahydroanthracenes and naphthalenes were classified as molecules having a similar reactivity. Hence, the hydrogenation reaction rates for dihydroanthracenes, biphenyls, tetrahydroanthracenes and naphthalenes are given by Eqs. (9)–(12). The monoaromatics hydrogenation reaction rates are also expressed in Eqs. (13)–(16). The formation of the 5 pseudo-components of saturates is also described in Eqs. (17)–(21):

$$r_{Dihydroanthracenes,n} = \left(k_{1_n} C_{Anthracenes,n} C_{H_2} - k_{-1_n} C_{Dihydroanthracenes,n} - k_{2_n} C_{Dihydroanthracenes,n} C_{H_2} + k_{-2_n} \frac{C_{Dinaphthenobenzenes,n}}{C_{H_2}^2}\right)\theta_\tau^2 \quad (9)$$

$$r_{Biphenyls,n} = \left(k_{5_n} C_{Alkyldibenzothiophenes,n} C_{H_2} + k_{6_n} C_{4\text{-}Alkyldibenzothiophenes,n} C_{H_2} - k_{2_n} C_{Biphenyls,n} C_{H_2} + k_{-2_n} \frac{C_{Cyclohexylbenzenes,n}}{C_{H_2}^2}\right)\theta_\tau^2 \quad (10)$$

$$r_{Tetrahydroanthracenes,n} = \left(-k_{3_n} C_{Tetrahydroanthracenes,n} C_{H_2} + k_{-3_n} \frac{C_{Dinaphthenobenzenes,n}}{C_{H_2}}\right)\theta_\tau^2 \quad (11)$$

$$r_{Naphthalenes,n} = \left(-k_{3_n} C_{Naphthalenes,n} C_{H_2} + k_{-3_n} \frac{C_{Tetralins,n}}{C_{H_2}} + k_{10_n} C_{Acridines,n} C_{H_2}\right)\theta_\tau^2 \quad (12)$$

$$r_{Dinaphthenobenzenes,n} = \left(k_{3_n} C_{Tetrahydroanthracenes,n} C_{H_2} - k_{-3_n} \frac{C_{Dinaphthenobenzenes,n}}{C_{H_2}} + k_{2_n} C_{Dihydroanthracenes,n} C_{H_2} - k_{-2_n} \frac{C_{Dinaphthenobenzenes,n}}{C_{H_2}^2} - k_{4_n} C_{Dinaphthenobenzenes,n} C_{H_2}\right)\theta_\tau^2 \quad (13)$$

$$r_{Tetralins,n} = \left(k_{3_n} C_{Naphthalenes,n} C_{H_2} - k_{-3_n} \frac{C_{Tetralins,n}}{C_{H_2}} - k_{4_n} C_{Tetralines,n} C_{H_2}\right)\theta_\tau^2 \quad (14)$$

$$r_{Benzenes,n} = (-k_{4_n} C_{Benzenes,n} C_{H_2} + k_{10_n} C_{Quinolines,n} C_{H_2} + k_{10_n} C_{Anilines,n} C_{H_2})\theta_\tau^2 \quad (15)$$

$$r_{Cyclohexylbenzenes,n} = \left(k_{2_n} C_{Biphenyls,n} C_{H_2} - k_{-2_n} \frac{C_{Cyclohexylbenzenes,n}}{C_{H_2}^2} - k_{4_n} C_{Cyclohexylbenzenes,n} C_{H_2} + k_{7_n} C_{4\text{-}Alkyldibenzothiophenes,n} C_{H_2} + k_{8_n} C_{4,6\text{-}Alkyldibenzothiophenes,n} C_{H_2}\right)\theta_\tau^2 \quad (16)$$

$$r_{Perhydroanthracenes,n} = (k_{4_n} C_{Dinaphthenobenzenes,n} C_{H_2})\theta_\tau^2 \quad (17)$$

$$r_{Perhydronaphthalenes,n} = (k_{4_n} C_{Tetralins,n} C_{H_2})\theta_\tau^2 \quad (18)$$

$$r_{Cyclohexanes,n} = (k_{4_n} C_{Benzenes,n} C_{H_2})\theta_\tau^2 \quad (19)$$

$$r_{Bicyclohexyls,n} = (k_{4_n} C_{Cyclohexylbenzenes,n} C_{H_2} + k_{9_n} C_{Carbazoles,n} C_{H_2})\theta_\tau^2 \quad (20)$$

$$r_{Para\,fins,n} = (k_{10_n} C_{Pyridines,n} C_{H_2})\theta_\tau^2 \quad (21)$$

3.2.4. Hydrodenitrogenation reactions

Regarding HDN, it has been reported in the literature that the main organic nitrogen family that is not completely converted are carbazoles [54–56]. The HDN of carbazoles and basic nitrogen compounds was both considered in the reaction scheme. Pyrroles and indoles are considered to be directly converted at the reactor inlet respectively into paraffins and cyclohexylbenzenes and ammonia. The rate determining step for HDN of carbazoles was assumed to be the first hydrogenation step of an aromatic cycle of the molecule. The hydrodenitrogenation rate equation can therefore be written as indicated in Eq. (22). Four kinds of basic pseudo-compounds (identified in Fig. 9 as NBAS), are hydrodenitrogenated according to four types of reactions to produce diaromatics, monoaromatics and saturated pseudo-compounds. The equations of HDN reaction rates are described in Eqs. (23)–(26):

$$r_{Carbazoles,n} = (-k_{9_n} C_{H_2} C_{Carbazoles,n})\theta_\tau^2 \quad (22)$$

$$r_{Pyridines,n} = (-k_{10_n} C_{H_2} C_{Pyridines,n})\theta_\tau^2 \quad (23)$$

$$r_{Quinolines,n} = (-k_{10_n} C_{H_2} C_{Quinolines,n})\theta_\tau^2 \quad (24)$$

$$r_{Acridines,n} = (-k_{10_n} C_{H_2} C_{Acridines,n})\theta_\tau^2 \quad (25)$$

$$r_{Anilines,n} = (-k_{10_n} C_{H_2} C_{Anilines,n})\theta_\tau^2 \quad (26)$$

The two denominators in the rate equations express the competitive adsorption of the various lumps on the hydrogenation and hydrogenolysis sites, and represents the fractions of free active sites (for hydrogenation and for hydrogenolysis) that are calculated as follows:

$$\theta_\tau = \left(1 + K_{H_2\tau} C_{H_2} + K_{NH_3\tau} C_{NH_3} + K_{SAT\tau} \sum_{i\in SAT} \sum_n C_{i,n} + K_{MONO\tau} \sum_{i\in MONO} \sum_n C_{i,n} + K_{DI1\tau} \sum_{i\in DI1} \sum_n C_{i,n} + K_{DI2\tau} \sum_{i\in DI2} \sum_n C_{i,n} + K_{TRI\tau} \sum_{i\in TRI} \sum_n C_{i,n} + K_{CARB\tau} \sum_{i\in CARB} \sum_n C_{i,n} + K_{NBAS\tau} \sum_{i\in NBAS} \sum_n C_{i,n} + K_{DBT2\tau} \sum_{i\in DBT2} \sum_n C_{i,n} + K_{DBT3\tau} \sum_{i\in DBT3} \sum_n C_{i,n}\right)^{-1} \quad (27)$$

$$\theta_\sigma = \left(1 + K_{H_2\sigma} C_{H_2} + K_{H_2S\sigma} C_{H_2S} + K_{NH_3\sigma} C_{NH_3} + K_{SAT\sigma} \sum_{i\in SAT} \sum_n C_{i,n} + K_{MONO\sigma} \sum_{i\in MONO} \sum_n C_{i,n} + K_{DI1\sigma} \sum_{i\in DI1} \sum_n C_{i,n} + K_{DBT1\sigma} \sum_{i\in DBT1} \sum_n C_{i,n} + K_{DBT2\sigma} \sum_{i\in DBT2} \sum_n C_{i,n}\right)^{-1} \quad (28)$$

Finally, the temperature dependence follows a classical Arrhenius law expression that has been reparameterized with respect to a reference temperature T_{ref}. To account for the variation of reactivity with carbon number, a LFER type relation based on the carbon number n is included, leading to the following expression:

$$k_{j_n}(T) = k_{j_0}(T_{ref}) e^{\alpha_j n} e^{[-E_j/R(1/T - 1/T_{ref})]} \quad (29)$$

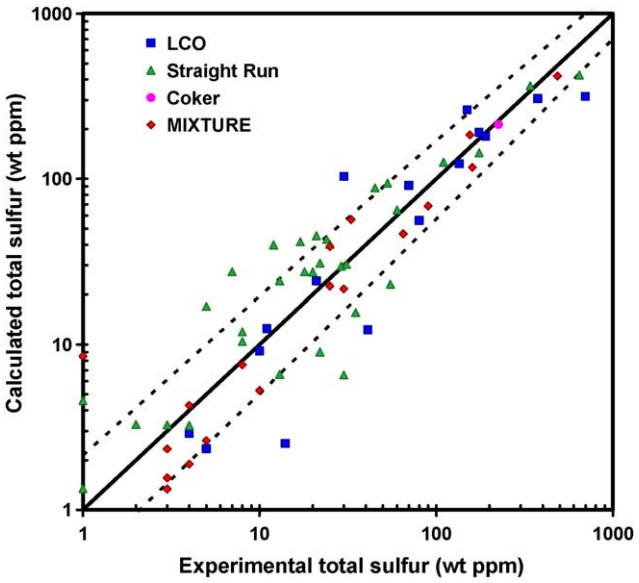

Fig. 12. Kinetic model results: comparison of calculated *vs.* experimental total sulfur content in hydrotreated products. Dotted lines correspond to the estimated sulfur that would be obtained if the reactor temperature was modified of ±5 °C.

3.3. Kinetic modeling results

The model parameter estimation was carried out using a Levenberg–Marquardt algorithm that minimizes a least squares objective function comparing the measured and predicted responses. The predicted responses were obtained by integrating the set of 597 differential equations of the model with a given set of parameters and grouping the predicted outlet concentrations into the lumps of the kinetic model. Concerning the measured responses, the database consisted of experimental results that were collected from 92 isothermal hydrotreating experiments in representative pilot plants. These data were acquired from the hydrotreatment of the 24 different feeds that were presented in the statistical reconstruction section. This means that the effluents were obtained from light cycle oils, straight run gas oils, coker gas oils as well as from the mixtures of these feeds. This feed diversity is particularly important to confer a high degree of robustness of the model and to be confident in its predictions.

The main results after optimization of the model parameters are shown in Figs. 12 and 13. Concerning the sulfur prediction, the 0–1000 wt ppm sulfur range is indicated. Dotted lines correspond to the estimated sulfur that would be obtained if the reactor temperature was modified of ±5 °C, the experimental pilot plant uncertainty corresponds to about 2–3 °C. As illustrated, there is no noticeable bias for the prediction of the residual total sulfur, neither by type of feed nor by sulfur content. Given the complexity of the chemical system as well as the experimental uncertainties of the pilot plant experimentation, the calculated sulfur content is reasonably close to the experimental values. It must be stressed that the properties of the hydrotreated products obtained from feed mixtures are also well predicted.

The aromatics prediction is illustrated in Fig. 13 in terms of the total aromatics, monoaromatics (MONO) and diaromatics + (-DI1 + DI2 + TRI) content. The total aromatics content is very well estimated: 86 from 92 effluents are predicted inside the ±5 wt.% interval (dotted lines). As indicated, the total aromatics content covers a wide range starting from 13 to 75 wt.%. Hence, the model is able to predict hydrotreating of feeds having a high content of aromatics, such as LCOs, as well as of mixtures or straight run gas oils. In conclusion, statistical reconstruction allow to provide detailed

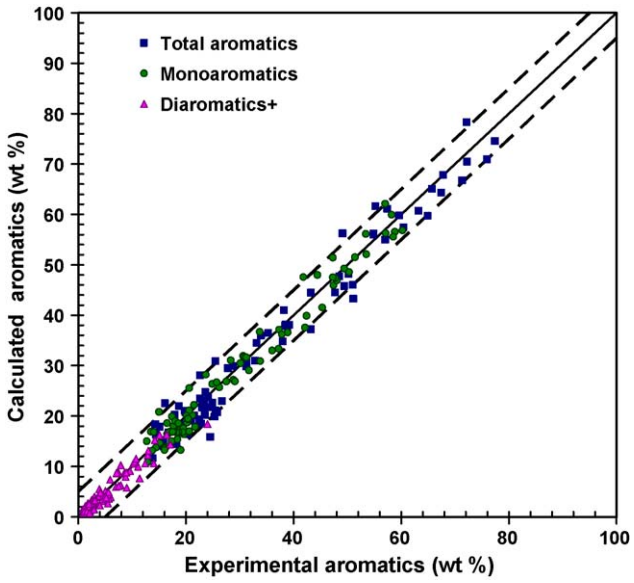

Fig. 13. Kinetic model results: comparison of calculated *vs.* experimental total aromatics, monoaromatics and diaromatics + content. Dotted lines, ±5 wt.%.

chemical information on gas oil fractions and is a very valuable tool to develop reliable and robust kinetic models as the one presented in this work.

4. Thermal stability analysis of a hydrotreatment reactor

Safety is one of the most important concerns in the chemical and refining industry. The thermal control of chemical reactors is an important issue for several reasons. The quality (conversions, selectivities) of the products to be manufactured generally depends considerably on reaction temperature. As chemical reactions exhibit an Arrhenius dependence on temperature, i.e., an exponential dependence, reactor temperature needs to be appropriately controlled. In the case of exothermic reactions, the loss of control of reactor temperature may eventually lead to a thermal runaway. Among the different consequences of a runaway, we can cite the loss of selectivity, degradation of the product quality, premature catalyst deactivation, increase of the reactor pressure, and even the loss of reactor integrity leading to major incidents and accidents.

Hydrotreating implies hydrogenation reactions that are highly exothermic. The content of unsaturated species in gas oils strongly depends on the operation or process from which they are obtained. Light Cycle Oils are produced from the Fluid Catalytic Cracking process, and contain a very high amount of unsaturated compounds, commonly above 70 wt.%. In industry, these gas oils are generally hydrotreated in small proportions mixed with straight run and other gas oils. The reason is not only the bad quality of these feeds (sulfur, cetane), but it is also a safety concern. Indeed, hydrotreating these feeds may lead to an excessive increase of reactor temperature or even a thermal runaway. Hence, the incorporation of higher amounts of highly reactive feeds requires not only to determine the most adequate operating conditions to obtain diesel products that achieve its specifications, but also to study the stability of the reactor from the thermal point of view. So, to ensure the operability and integrity of the reactor, a method to determine *a priori* the behavior of the reactive system is necessary. Indeed, small perturbations of the parameters of the system may lead to slight changes in the process variables such as temperature, but radical changes of the system can also be observed, however. In this work, the "stability" study intends to tackle the thermal state and to determine *a priori* for a given set of operating conditions if the reactor will stay at the same thermal level when the system is perturbed. Hence, the objective is to dispose of theoretical methods to determine in a reliable way whether the system is thermally stable or not. An extensive number of literature works have discussed the reactor stability topic. van Heerden [10] presented an approach where the thermal balance equation is arranged to represent the heat generated per total heat capacity of the reactor (Q_{gen}) and a curve of the heat removal by flow and heat transferred (Q_{trans}). Both heats are represented as two curves in a diagram; the heat balance is solved for the temperature variable and the intersection of both curves corresponds to the steady-state operating point. Another concept related to the stability of chemical reactors was exposed by Bilous and Amundson [57]. They explain that there are regions of operation where small changes of the parameters of the system produce large alteration of the variables. In such cases, the reactor is said to exhibit a parametric sensitivity behavior. In other words, parametric sensitivity consists of determining the regions where the reactive system is very sensitive to small changes of the inlet parameters. The parametric sensitivity analysis has been largely adopted to determine the thermal stability of reactive systems [58–66]. This analysis has generally been carried out for steady-state conditions for different types of reactive systems. Various sensitivity criteria have been developed for several types of reactors such as batch [58,59], CSTR [60], pseudo-homogeneous tubular reactors [61–63], and fixed-bed catalytic reactors [64–68]. This kind of approach allows to determine for example the normalized sensitivities that help to identify the region where the system operation becomes unreliable. Another application is to trace runaway/non-runaway maps. In studies concerning fixed-bed reactors, the role of intra- and inter-particle transfer limitations has been studied. Some works concerning catalytic fixed-bed reactors deal with the study of flow maldistributions which can bring about hot spot formation. Other studies [69,70] present a procedure to calculate the critical residence time at which runaway occurs. The experimental study of hot spots in packed-bed reactors has also been reported [67,68]. Concerning the dynamic stability analysis, the development of an intrinsic criterion based on the sum of Lyapunov exponents is presented in several literature works [71,72] where the instabilities are characterized with chaotic attractors. These studies have been carried out in batch and semi-batch reactors. The perturbation stability analysis and the chaos theory has more recently been extended to deal with the determination (1D or 2D) of hot spots in packed-bed reactors [73–75]. Most of the models study the instabilities in homogeneous or pseudo-homogeneous systems with relatively simple reaction networks. The contribution of our work consists in carrying out a thermal stability analysis of a hydrotreating pilot plant working at industrial operating conditions with actual feeds. Opposed to most literature works where the reactive systems are represented *via* pseudo-homogeneous models, this study uses a heterogeneous model accounting for the presence of solid, liquid and vapor phases. A dynamic reactor model was developed based on experimental data and adapted to this complex reactive system. This model was used to perform a thermal stability analysis at stationary conditions, but also according to its transient behavior.

4.1. Theoretical aspects

4.1.1. Steady-state stability

The stability of operation of chemical reactors at stationary conditions is based on the van Heerden criterion [10]. The principle is also extensively described by Froment and Bischoff [76]. This criterion imposes that the slope of heat generated by the reactions

must be lower than the slope of the heat transferred through the wall. This can be expressed as

$$\frac{dQ_{gen}}{dT} < \frac{dQ_{trans}}{dT} \tag{30}$$

The comparison between both slopes is generally represented as a stability diagram. Two representations are commonly used. The first one consist to plot both heats (Q_{gen} and Q_{trans}) as a function of temperature. In the case of a stationary stable reactor, there must be only one intersection of both curves and the intersection point corresponds to the operating point. If the operating conditions are perturbed, two cases can be considered. The condition imposed in Eq. (30) is satisfied and the system will return to its original state which corresponds to a stable stationary equilibrium. Otherwise, Eq. (30) is not satisfied and it will be possible to observe a multiplicity of steady-states for a given set of operating conditions. The most classic case corresponds to three possible steady-states, the middle point is unstable and depending on the direction of the perturbation, the operating point will change and converge to one of the other steady-states. The lowest temperature point corresponds to the extinguish point and highest temperature corresponds to an ignition point which may lead to a thermal runaway. The second representation of the stability curve consists in plotting the reactor temperature as a function of the cooling temperature or inlet temperature. To satisfy the steady-state stability, for a given cooling or inlet temperature, only one reactor temperature must be obtained. For unstable reactors, an "*S*" curve will be obtained. Consequently, three reactor temperatures will be possible for a given cooling or inlet temperature. A hysteresis behavior is then observed. This representation will be referred to as a hysteresis diagram. The stationary analysis is useful to identify a preliminary stable/unstable region or to determine for a given equilibrium point if it is stable or not.

4.1.2. Stability under transient conditions

Since the steady-state stability analysis is only performed under stationary conditions, the dynamic behavior of the system is not taken into account and the thermal stability cannot be guaranteed. The steady-state condition is necessary condition to ensure the thermal stability, but it is not a sufficient condition. This means that stable stationary zones are not granted to be stable in the dynamic stability analysis. This is obviously due to the fact that accumulation terms are not taken into account in the static analysis.

The dynamic stability analysis is carried out by perturbing the operating variables [77] and is composed of the following main steps: (a) integration of the dynamic equations in the axial direction using a numerical scheme, (b) perturbation of the dynamic reactor model, (c) linearization of the perturbation model and (d) resolution of the perturbation model and (e) analysis of the solution. The condition for stability implies that all perturbations must tend to be zero when time tends to infinity [76]. The next paragraph describes these steps in more detail.

The first step is the integration of the model. The integration along the z axis is carried out using an upwind scheme for the convective terms and a centered scheme for the diffusion–dispersion terms. The reactor model can be written in a matrix formalism as follows:

$$\frac{\partial \vec{y}}{\partial t} = \vec{f}(\vec{y}) \tag{31}$$

where $\vec{y}$ is the variables vector and $\vec{f}$ is the vector of the second member of partial differential equations.

The variable vector $\vec{y}$ is perturbed by an amount of vector $\vec{x}$ around an equilibrium point as follows:

$$\vec{y}_p = \vec{y} + \vec{x} \Rightarrow \vec{x} = \vec{y}_p - \vec{y} \tag{32}$$

Since the applied perturbations are very small, a first-order Taylor expansion can be applied to linearize the reactor model around the stationary point, and the perturbation model can be expressed as

$$\frac{\partial x_i}{\partial t} = \left(\frac{\partial f_i}{\partial y_1}\right)_{op} x_1 + \left(\frac{\partial f_i}{\partial y_2}\right)_{op} x_2 + \ldots + \left(\frac{\partial f_i}{\partial y_i}\right)_{op} x_i + \ldots + \left(\frac{\partial f_i}{\partial y_n}\right)_{op} x_n \tag{33}$$

Hence, the perturbation model can be written as a matrix (Eq. (34)), where **J** is the Jacobian of $\vec{f}$:

$$\frac{\partial \vec{x}}{\partial t} = \mathbf{J}\vec{x} \tag{34}$$

The resolution of this linear system of first-order differential equations allows to assess whether the perturbation of at least one of the whole set of variables diverges with time and propagates. In this case, the system will not return to its initial steady-state before the perturbation and the reactor will have an unstable behavior. The solution of the perturbation around the stationary point is given by Eq. (35), where $\vec{V}$ designates the eigenvectors of the Jacobian and λ_j its eigenvalues:

$$x_i = \sum_j V_{i,j} a_j e^{\lambda_j t} \tag{35}$$

Eigenvalues can be real (**R**) or complex (**C**). The stability condition (Eq. (35)) imposes that all eigenvalues must have a negative real part. Indeed, even if only one eigenvalue is positive, all perturbations x_i will tend to infinity when time increases. If the eigenvalues have an imaginary part (**C**), an oscillatory behavior will be observed, which may remain constant, be attenuated or be amplified depending on the sign of the real part of the eigenvalues.

For the hydrotreating of Light Cycle Oils, both the stationary and dynamic stability analyses were performed.

4.2. Dynamic HDT reactor model

A reactor model was developed for the thermal stability study presented in this section. This model was built on the basis of an existing pilot plant (Fig. 14), taking into account the actual reactor configuration (geometry, flow streams, heaters, control system) to accurately represent the reactor behavior. The material and thermal balance equations describe the three-phase system. The working hypotheses for the development of the model are described in the next paragraphs.

The kinetic model described in Section 2 is intended to be used to accurately predict the detailed performances of the process such as very low residual sulfur levels or the detailed composition of hydrocarbon families to predict product properties such as cetane number or density. As explained above, the corresponding steady-state simulations are performed by integrating the set of 597 differential equations. For thermal stability purposes, the main objective of the kinetic model is to correctly assess the source term to estimate the heat released by reactions. Hence, it is not required to precisely predict the evolution of impurities such as sulfur and nitrogen, which will no longer contribute to the heat release. In order to cope with computational burden of the dynamic stability analysis, a reduced kinetic model was therefore developed. In a first step, the break-down by carbon number was modified. In the reduced kinetic model used in this section, only three boiling point (BP) fractions were considered for the chemical lumps: (1)

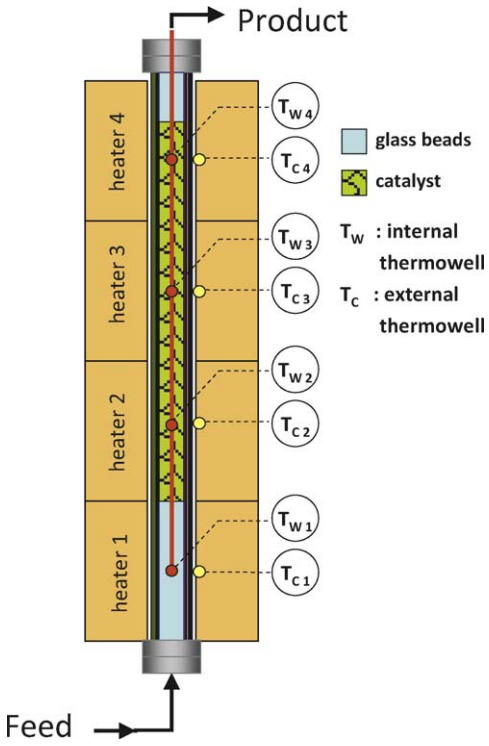

Fig. 14. Scheme of the LCO hydrotreating reactor.

Table 3
Description of hydrocarbon lumps in the kinetic scheme used for the thermal stability study.

Lump	BP cut 1: IBP-200 °C	BP cut 2: 200–300 °C	BP cut 3: 300 °C+
TRI			X
DI		X	X
MONO	X	X	X
SAT	X	X	X
SULFUR	X	X	X
OLEFINS	X	X	X

IBP-200 °C, (2) 200–300 °C and (3) 300 °C+ (Table 3). This allowed to reduce the number of differential equations that needed to be solve in space and time, while three BP cuts were found to be representative enough to describe the vapor–liquid distribution of the reactive system. Secondly, the number of lumps was also reduced. All sulfur compounds were lumped together into a SULFUR group. Hydrodenitrogenation reactions were neglected here since the amounts of nitrogen in gas oil feeds are very low and their contribution to the source term is also very low. Diaromatics were considered to be a unique lump. The triaromatics are hydrogenated to form diaromatics (TRI + $2H_2 \rightarrow$ DI). Diaromatics are hydrogenated into monoaromatics (DI + $2H_2 \rightarrow$ MONO), which are also obtained from the hydrodesulfurization of sulfur compounds (SULFUR + $5H_2 \rightarrow$ MONO + H_2S). Monoaromatics are further hydrogenated into saturates (MONO + $3H_2 \rightarrow$ SAT). For simplifying purposes in this study, aromatics hydrogenation was considered to be irreversible, however, reversibility of reactions will be taken into account in future work. A lump of olefins was added to the reaction scheme to form saturates (OLEF + $2H_2 \rightarrow$ SAT). Olefins must be considered since LCO feeds contain about 5–10 wt.% of these compounds. Moreover, this chemical family has a high reactivity. It is essentially converted at the reactor inlet and its contribution to the heat release is important, for this reason, they were included in the reduced kinetic scheme. The reaction rates were considered to follow a power law as expressed in Eq. (36). The catalyst was considered to be completely wetted, as the pilot plant was operated in upflow mode. Hence, the reactions are supposed to be carried out only in the liquid phase:

$$r_j = k_{j_0} C_{l_m}^{a_j} C_{l_{H_2}}^{b_j} \exp\left[-\frac{E_j}{R}\left(\frac{1}{T}-\frac{1}{T_{ref}}\right)\right] \quad (36)$$

where j designates the reaction index, k_{j_0} is its rate constant at a reference temperature T_{ref}, E_j is its activation energy, C_{l_m} is the liquid concentration of hydrocarbon family m, and $C_{l_{H_2}}$ is the liquid concentration of hydrogen. The reactivity of each hydrocarbon lump was supposed to be independent of the BP cut. The parameters of this reduced kinetic model were estimated on the basis of 49 experimental pilot plant points obtained with six different industrial LCO feeds. The experimental points were all obtained from HDT experiments carried out in the industrial range of operating conditions. The kinetic model results give a very good estimate of the hydrotreating reactions. Monoaromatics are mainly predicted within the ±5 wt.% interval (82% of the points); for diaromatics 86% of points are predicted at ±3.5 wt.%. As expected, with this simplified model, HDS predictions are less accurate than the model in Section 2. However, the sulfur values correspond to trace levels and their impact on the thermal balance and stability analysis is not critical.

The other considerations of the reactor model are as follows. All the compounds (H_2, H_2S) and hydrocarbon lumps in the gas and liquid are considered to be in equilibrium. The liquid flow is described by an axial dispersion model, while the gas flow is considered to be in plug-flow. The gas holdup is assumed to be constant all along the reactor due to the low consumption of hydrogen compared to the inlet flow rate (hydrogen is added in large excess). The pressure drop is negligible compared to the total pressure, therefore, the reactor was considered to be isobaric. Liquid–solid external mass transfer limitations and internal diffusion limitations are also neglected, and are therefore included into the apparent kinetics. The superficial liquid velocity is considered to be constant along the reactor. Indeed, there are no cracking reactions and the liquid density remains almost constant between the reactor inlet and the reactor outlet. Since the heat transfers between all phases are very high, gas, liquid and solid are considered to be at the same temperature at a given axial coordinate (no radial dispersion).

With these model assumptions, the material balance for each hydrocarbon lump is given by Eq. (37):

$$\frac{\partial(\varepsilon_g C_i^g + (\varepsilon_l + \varepsilon_s\varepsilon_{por})C_i^l)}{\partial t} = -u_l\varepsilon_l\frac{\partial C_i^l}{\partial z} - \varepsilon_g\frac{\partial(u_g C_i^g)}{\partial z} + D_{ax}^l\varepsilon_l\frac{\partial^2 C_i^l}{\partial z^2} + \sum_j \mu_{ij} r_j \varepsilon_s \rho_s \quad (37)$$

Since the gas and liquid phases are considered to be in equilibrium, the concentrations in both phases for each lump are related by a Henry law. With this consideration, Eq. (37) can be rewritten as

$$\frac{\partial C_i^l}{\partial t}\left(\varepsilon_g\frac{H_i}{RT} + \varepsilon_l + \varepsilon_s\varepsilon_{por}\right) = -\frac{C_i^l}{R}\varepsilon_g\frac{\partial(H_i/T)}{\partial t} + D_{ax}^l\varepsilon_l\frac{\partial^2 C_i^l}{\partial z^2} - u_l\varepsilon_l\frac{\partial C_i^l}{\partial z} - \varepsilon_g\frac{\partial(u_g(C_i^l H_i/RT))}{\partial z} + \sum_j \mu_{ij} r_j \varepsilon_s \rho_s \quad (38)$$

The gas velocity changes all along the reactor due to the temperature profile, H_2 consumption and H_2S production and the partial vaporization of the hydrocarbon lumps. To be able to calculate this variable, the transient material balances (Eq. (37)) are summed for all hydrocarbon lumps. Converting the gas concentrations into partial pressures allows to introduce the

constraint of constant total pressure. In this way, the variation of gas velocity can be obtained from the following expression:

$$\frac{\partial(u_g/T)}{\partial z} = \frac{R}{\varepsilon_g P_t}\left(-(\varepsilon_l + \varepsilon_s\varepsilon_{por})\frac{\partial\sum_i C_i^l}{\partial t} + D_{ax}^l\varepsilon_l\frac{\partial^2\sum_i C_i^l}{\partial z^2} - u_l\varepsilon_l\frac{\partial\sum_i C_i^l}{\partial z} + \frac{\varepsilon_g P_t}{R}\frac{1}{T^2}\frac{\partial T}{\partial t} + \sum_i\sum_j \mu_{ij} r_j \varepsilon_s \rho_s \right) \quad (39)$$

The thermal balance is shown in Eq. (40). Accumulation terms for the gas, the liquid, the solid catalyst and the metallic mass of the reactor are taken into account. A heat transfer term is also considered to describe the heat loss through the reactor wall.

$$\frac{\partial T}{\partial t}\left(\varepsilon_g C p_g \rho_g + \varepsilon_l C p_l \rho_l + \varepsilon_s C p_s \rho_s + \frac{S_w}{S_r} C p_{steel}\rho_{steel}\right) = \varepsilon_l\frac{\partial}{\partial z}\left(\bar{\lambda}_{ax}\frac{\partial T}{\partial z}\right) - (\rho_l C p_l \varepsilon_l u_l + \rho_g C p_g \varepsilon_g u_g)\frac{\partial T}{\partial z} + \sum_j r_j \varepsilon_s \rho_s (-\Delta H_j) - U_{wall}A_{wall}(T - T_C) \quad (40)$$

In total, the state variables of the dynamic reactor model are the liquid concentrations of the 17 lumps (hydrocarbons + H_2 + H_2S) of the reduced kinetic scheme and the temperature.

The four electric heaters (Fig. 14) were also modeled. The internal reactor temperature is controlled by regulating the temperature of the thin layer of air located between the reactor and the heaters. This air can be warmed up by an electrical resistance. The transient thermal balance of the air layer is described by Eq. (41). The heat losses through the isolated device are also taken into account.

$$\rho_{air} C p_{air}\frac{\partial T_C}{\partial t} = -\rho_{air} C p_{air} u_{air}\frac{\partial T_C}{\partial z} + U_{wall}A_{wall}\frac{S_r}{S}(T - T_C) - U_{loss}A_{wall}\frac{S_r}{S}(T_C - T_{amb}) + \frac{Q_k}{Sh_{heater,k}} \quad (41)$$

The control of the heaters is described through Eq. (42). Each controller has its own temperature setpoint ($T_{set,k}$) in relation to the corresponding internal temperature measurement ($T_{W,k}$):

$$\frac{\partial Q_k}{\partial t} = G(T_{set,k} - T_{T_{W,k}}) - \tau_{cont}\frac{\partial T_{T_{W,k}}}{\partial t} \quad (42)$$

Since it is essential to validate the dynamic model used for the thermal stability study, an experiment was carried out in order to collect transient temperature data (Fig. 15). After hydrotreating a straight run gas oil at 300 °C, a LCO was fed into the reactor (time = 0). This change of feed resulted in an increase of the reactor temperature profile. Temperatures of the four internal thermocouples were recorded and compared to the temperatures predicted by the model at the axial coordinates where the thermocouples are located inside the thermowell. As illustrated in Fig. 15, the model predictions agree very well with the experimental temperatures observed after injection of the LCO. Hence, these results validate the reactor model with its reduced kinetic scheme as basis for the thermal stability study.

4.3. Thermal stability analysis results

The stationary stability analysis was carried out for the LCO hydrotreating unit. The hysteresis curve was adopted to represent the stationary stability analysis. The average temperature along the reactor was obtained by imposing a constant cooling temperature (T_c) along the z axis. In this case, the regulation was performed according to Eq. (43):

$$\frac{dT_c}{dt} = \kappa_{control}(T_{mean\_set} - T_{mean}) - \tau_{control}\frac{dT_{mean}}{dt} \quad (43)$$

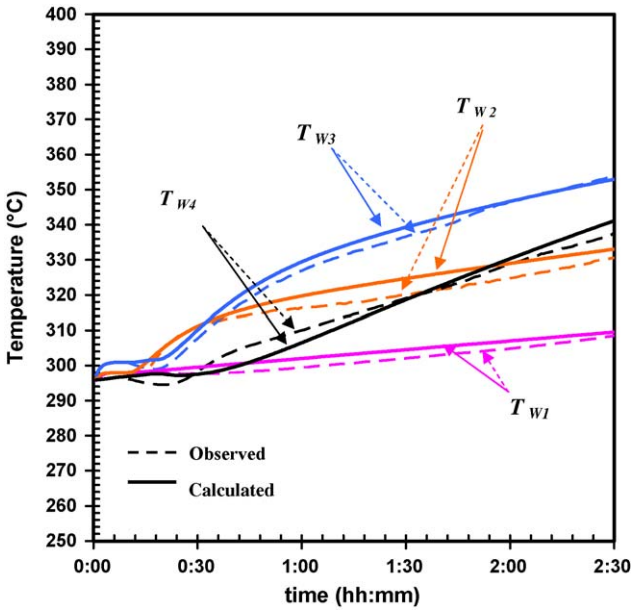

Fig. 15. Comparison between experimental and calculated transient temperatures of the HDT pilot plant.

where T_{mean_set} is the average reactor temperature setpoint, T_{mean} is the actual average reactor temperature and $\kappa_{control}$ and $\tau_{control}$ are the proportional and derivative control parameters, respectively. Under normal operating conditions, no unstable behavior was identified: a monotonous hysteresis steady-state diagram is obtained. For purposes of this study, the operating conditions were deliberately imposed in a severe zone in order to look for an unstable domain. The conditions tested are as follows: feed = 100% LCO, U_{wall} = 3 W/m^2/K, P = 150 bar, T_{inlet} = 200 °C and LHSV = 1.1 h^{-1}. The data to trace the hysteresis curve were calculated with these conditions. The stationary equilibrium points for an average reactor temperature going from 200 °C to 376 °C were calculated with increments of 2 °C. Fig. 16 shows that a hysteresis curve is clearly observed. In the T_{mean} range between 263 °C and 323 °C the reactor has an unstable behavior. The operating points inside this range cannot be attained without a

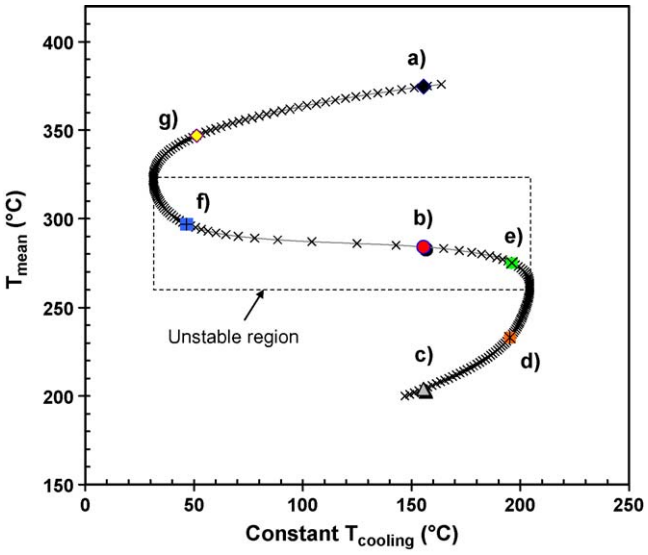

Fig. 16. Hysteresis stability curve of LCO pilot plant hydrotreatment at severe conditions.

Table 4
Dynamic stability results: highest eigenvalues of different stationary points.

Case	T_{mean} (°C)	$T_{cooling}$ (°C)	Highest eigenvalue (real part)
(d)	233.00	195.15	-1.57×10^{-5}
(e)	275.00	196.11	2.40×10^{-5}
(f)	297.00	46.55	2.01×10^{-5}
(g)	347.00	51.27	-1.01×10^{-4}

control system. Actually, inside this range, the operation of the reactor is unreliable: if the control system shuts down, the operating point will change to the upper or lower curve branches, which correspond to the ignition and extinction curves respectively. In the case of a jump to a quench point, the desired reactions will no longer be carried out at their target conversion and the product will not have the desired specifications. In the case of a jump to an ignition point, the catalyst may be prematurely deactivated, some undesired reactions may start, and this situation can eventually lead to a runaway. An example is indicated as points (a), (b) and (c) in the same figure. If the reactor has to operate at point (a) and the control system has a failure, at the same cooling temperature, a perturbation of the inlet parameters of the system will shift the operation point of the reactor either to point (b) or point (c), which are both stable operating points. By performing dynamic simulations at these conditions, both scenarios could be reproduced, confirming the results obtained with stationary stability analysis.

The same system was studied according to the dynamic stability analysis. The model equations were discretized in 50 spatial steps (nz). As described before, the reactor model variables are the liquid concentrations of the 17 lumps (feedstock + H_2 + H_2S) and the temperature at each axial coordinate. Hence, the dimension of each of the $\vec{y}$, $\partial\vec{y}/\partial t$ and $\vec{f}$ vectors is 900. In the $\vec{y}$ vector, the first 850 lines correspond to the liquid concentrations of the 17 lumps at each axial coordinate (17×50). The last 50 lines correspond to the temperature at each spatial step. An analog reasoning can be made for the transient vector $\partial\vec{y}/\partial t$. The first 850 lines of the $\vec{f}$ vector correspond to the second member of the material balance (MB) for each lump at each axial coordinate in the reactor. The last 50 lines contain the second member of the thermal balance (TB) at each spatial step. Therefore, the Jacobian (**J**) of the application $\vec{f}$ is a matrix of dimension 900×900.

The dynamic stability analysis was performed for points (d), (e), (f) and (g) from Fig. 16. The procedure indicated in Section 4.1.2 was applied for each point. The results are summarized in Table 4. For each case, the highest real part of the eigenvalues is listed in this table. According to the dynamic stability criterion, the real part of all eigenvalues must be negative, otherwise the system is unstable. As indicated, operating points (d) and (g) are stable while points (e) and (f) are unstable. Fig. 17 illustrates the spectrum of the 900 eigenvalues of case (f) that corresponds to T_{mean} = 297 °C and a constant axial cooling temperature of 46.6 °C. The abscissa indicates the real part of the eigenvalues, and the y coordinate is the imaginary part. As illustrated, only one eigenvalue has a positive real part, but this is enough to make the system unstable. Fig. 18 corresponds to the eigenvalues of case (g) corresponding to a T_{mean} = 347 °C. This stationary point is dynamically stable since

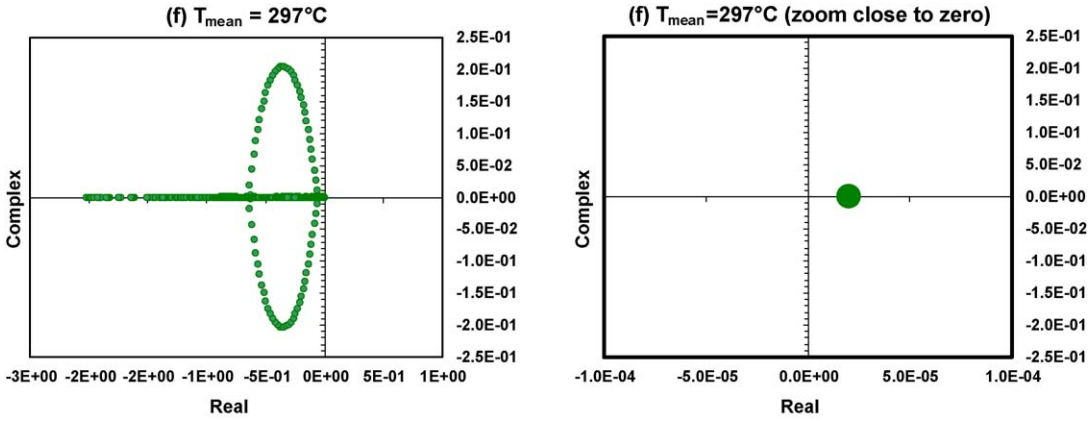

Fig. 17. Spectra of eigenvalues of case (f) T_{mean} = 297 °C and the corresponding zoom close to zero.

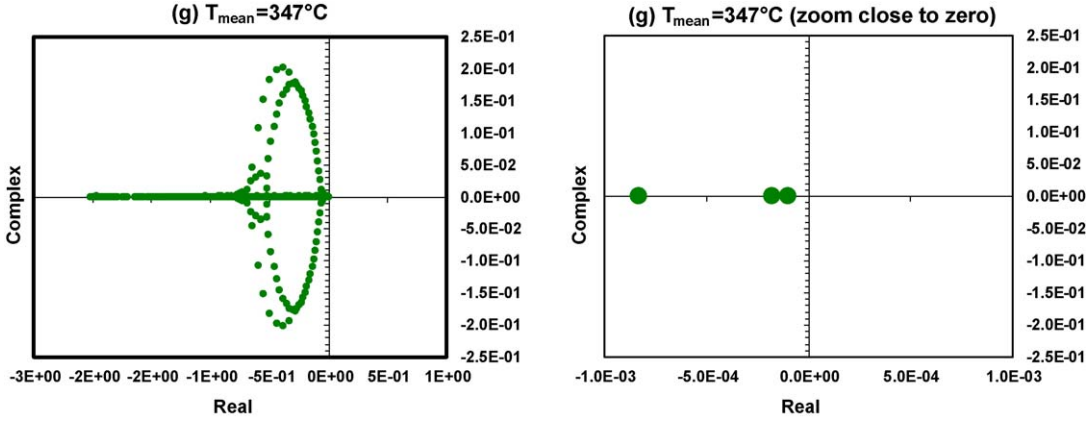

Fig. 18. Spectra of eigenvalues of case (g) T_{mean} = 347 °C and the corresponding zoom close to zero.

all eigenvalues are negative. The form of both spectra is also different. As shown in this part of the work, the analysis of the eigenvalue spectrum allows to determine whether the system is stable or unstable.

The methodology presented here to study the thermal stability of exothermic systems is particularly interesting to ensure the safe range of operating conditions of existing and also new processes (e.g., the hydrotreatment of biodiesel) or even for revampings. This method can be applied for the stability analysis of pilot plants and even of industrial units provided that the reactor model represents the actual reactive system.

5. Conclusions

This work presents a summary of the modeling approach developed to study the gas oil hydrotreating process. Our approach covers the detailed quantitative description of gas oils *via* a novel statistical reconstruction method. This gas oil characterization was subsequently used to develop a predictive kinetic model that is able to estimate the HDT performances of various types of feeds under industrial operating conditions. Since HDT reactions are highly exothermic, this work was completed by developing a procedure to perform a stationary and a dynamic thermal stability analysis that was applied to a HDT pilot plant. The steps of this procedure can be applied to study other HDT plants (even industrial units), provided that another reactor model adapted to predict the plant to be studied is developed.

The statistical reconstruction method enables to calculate the gas oil composition by carbon number (C_1 to C_{30}) and by chemical family (28) including saturates, aromatics and heteroatomic hydrocarbons (S, N). This tool provides a detailed characterization of these complex hydrocarbon fractions using only some analyses: mass spectrometry, sulfur speciation, nitrogen speciation and simulated distillation. Such a characterization, which comprises 597 pseudo-compounds, would be very difficult to obtain without this reconstruction method. The properties of each pseudo-compound are calculated by inspection or by using group contribution methods. Mixing rules are applied to determine the mixture properties for each gas oil by combining the pseudo-compounds properties and the matrix composition. The statistical reconstruction results were compared to the actual analyses for various kinds of gas oils (straight run, LCO, coker). An excellent agreement between calculated and experimental properties was obtained. These results are extremely encouraging and provide valuable detailed information on gas oil compositions.

Using the statistical reconstruction information, a kinetic model for the hydrotreating of full-range industrial gas oil feeds was developed. The kinetic model is based on a reaction scheme with a break-down by carbon number, and includes all hydrotreating reactions (hydrodesulfurization, hydrodearomatization and hydrodenitrogenation). A Langmuir–Hinshelwood representation was adopted to take into account the inhibiting effect of aromatics and nitrogen species on HDS. The detailed sulfur speciation analysis of gas oil feeds and of their hydrotreated products were used to better understand the reactivity of refractory sulfur compounds in industrial feeds. A first-order kinetic analysis of individual dibenzothiophenes allowed to differentiate three reactivity groups of dibenzothiophenes, thereby improving the accuracy of HDS performance predictions. The parameters of the model were fitted on the basis of hydrotreating experiments performed in a pilot plant using an industrial $NiMo/Al_2O_3$ catalyst working under industrial operating conditions. A very good agreement was obtained between the experimental and predicted yields of the hydrocarbon families. For residual sulfur contents, a relative good accuracy was obtained. It must be stressed that the model is not only reliable but also has a very high degree of robustness, since it is adapted to various types of feeds such as SR gas oils, LCO feeds, coker gas oils, as well as their mixtures.

Finally, the thermal stability analysis of a hydrotreating LCO pilot plant was performed. For this purpose, a dynamic model of the pilot plant reactor was developed. The model takes into account a detailed description of the reactive system and the configuration of the pilot plant: the three phases (gas–liquid–solid), the kinetics, the flow characterization in the gas and liquid phases, the heating devices and the control system. An experimental test was carried out to collect dynamic data for the validation of the model.

The thermal stability analysis of LCO hydrotreating was performed according to stationary and dynamic criteria. A hysteresis curve was obtained for extremely severe operating conditions that clearly delimited an unstable operating region. The perturbation method was also presented and applied to compare stationary and dynamic criteria. The dynamic criterion of stability imposes that after the solution of the perturbation system, all the resultant eigenvalues must have a negative real part, otherwise the reactor will be unstable. The thermal stability methodology presented in this work can be applied for an industrial reactor model fitted using industrial data. The usefulness would be to determine whether a unit can safely process a higher quantity of very reactive feeds such as LCO or Coker gas oil.

Several improvements of this integrated modeling approach are currently underway. For the statistical reconstruction, the IBP and FBP of the SimDist need to be calculated in a more accurate manner. It would also be useful to develop new group contribution methods to estimate other major diesel fuel properties such as viscosity or cetane index. Concerning the kinetic model, the HDS prediction could be still improved. Indeed, it would also be interesting to include different studies concerning the inhibiting effects of various organic nitrogen families. Finally, concerning the thermal stability analysis, further information can be obtained, such as the determination of stable/unstable maps, or the study of possible oscillatory reactor behavior. Other aspects such as the interpretation of the eigenvectors (location of instabilities) and the influence of other numerical aspects (solution scheme, Jacobian accuracy) will also be studied in the future.

References

[1] C. López-García, et al. Anal. Chem. 74 (2002) 3849–3857.
[2] N. Revellin, "Modélisation cinétique de l'hydrotraitement des distillats sous-vide", PhD Thesis, Claude Bernard Lyon I University, France, 2006.
[3] N. Revellin, et al. Energy Fuel 19 (2005) 2438–2444.
[4] R. Ruiz-Guerrero, et al. J. Chromatogr. Sci. 44 (2006) 566–573.
[5] F. Adam, et al. J. Chromatogr. A 1148 (2007) 55–64.
[6] C. Vendeuvre, et al. J. Chromatogr. A 1086 (2005) 21–28.
[7] F. Adam, et al. J. Chromatogr. Sci. 45 (2007) 643–649.
[8] H. Castex, et al. Rev. Inst. Fr. Petrol. 38 (1983) 523–532.
[9] A. Fafet, et al. Oil Gas Sci. Technol. 54 (1999) 439–452.
[10] C. van Heerden, Ind. Eng. Chem. 45 (1953) 1242–1247.
[11] D.K. Liguras, D.T. Allen, Ind. Eng. Chem. Res. 28 (1989) 665–673.
[12] D.K. Liguras, D.T. Allen, Ind. Eng. Chem. Res. 28 (1989) 674–683.
[13] R.J. Quann, S.B. Jaffe, Ind. Eng. Chem. Res. 31 (1992) 2483–2497.
[14] R.J. Quann, S.B. Jaffe, Chem. Eng. Sci. 51 (1996) 1615–1635.
[15] Y. Zhang, "A Molecular Approach for Characterization and Property Predictions of Petroleum Mixtures with Applications to Refinery Modelling", PhD Thesis, University of Manchester, United Kingdom, 1999.
[16] M. Neurock, "A Computational Chemical Reaction Engineering Analysis of Complex Heavy Hydrocarbon Reaction Systems", PhD Thesis, University of Delaware, USA, 1992.
[17] M. Neurock, et al. Chem. Eng. Sci. 49 (1994) 4153–4177.
[18] D.M. Trauth, "Structure of Complex Mixtures through Characterization, Reaction, and Modeling", PhD Thesis, University of Delaware, USA, 1993.
[19] D.M. Trauth, et al. Energy Fuel 8 (1994) 576–580.
[20] D. Hudebine, "Reconstruction moléculaire de coupes pétrolières", PhD Thesis, École Normale Supérieure de Lyon, France, 2003.
[21] D. Hudebine, J.J. Verstraete, Chem. Eng. Sci. 59 (2004) 4755–4763.
[22] K.M. Van Geem, et al. Comput. Chem. Eng. 31 (2007) 1020–1034.
[23] A. Fafet, J. Magné-Drisch, Rev. Inst. Fr. Pétrol. 50 (1995) 391–404.
[24] M. Houalla, et al. J. Catal. 61 (1980) 523–527.
[25] T. Kabe, et al. Appl. Catal. A-Gen. 97 (1993) L1–L9.

[26] T. Isoda, et al. Symp. on advances of hydrotreating catalysts, 208th National Meeting, American Chemical Society, Washington, (1994), pp. 584–586.
[27] G.F. Froment, et al. Ind. Eng. Chem. Res. 33 (1994) 2975–2988.
[28] M.V. Landau, et al. J. Catal. 158 (1996) 236–245.
[29] G.F. Froment, et al. in: Proceedings of the 1st International Symposium/6th European Workshop (Belgium), 1997, pp. 83–97.
[30] V. Vanrysselberghe, G.F. Froment, Ind. Eng. Chem. Res. 37 (1998) 1235–1242.
[31] T. Kabe, et al. Sekiyu Gakkaishi 42 (1999) 150–156.
[32] W.R.A.M. Robinson, et al. Fuel Process. Technol. 61 (1999) 89–101.
[33] G.F. Froment, Catal. Today 98 (2004) 43–54.
[34] P. Zeuthen, et al. Catal. Today 65 (2001) 307–314.
[35] G.C. Laredo, et al. Appl. Catal. A-Gen. 207 (2001) 103–112.
[36] T. Koltai, et al. Appl. Catal. A-Gen. 231 (2002) 253–261.
[37] G.C. Laredo, et al. Appl. Catal. A-Gen. 243 (2003) 207–214.
[38] D. Ferdous, et al. Energy Fuel 17 (2003) 164–171.
[39] T.C. Ho, D. Nguyen, J. Catal. 222 (2004) 450–460.
[40] V. Rabarihoela-Rakotovao, et al. Appl. Catal. A-Gen. 237 (2004) 17–25.
[41] P. Steiner, E.A. Blekkan, Fuel Process. Technol. 79 (2002) 1–12.
[42] R.M. Cotta, et al. Comp. Chem. Eng. 23 (1999) S791–S794.
[43] R. Chowdhury, et al. AIChE J. 48 (2002) 126–135.
[44] E. Pedernera, et al. Catal. Today 79–80 (2003) 371–381.
[45] A. Owusu-Boakye, et al. Ind. Eng. Chem. Res. 44 (2005) 7935–7944.
[46] J. Chen, et al. Petrol. Sci. Technol. 21 (2003) 911–935.
[47] J.W. Chen, et al. Catal. Today 98 (2004) 227–233.
[48] A. Al-Barood, et al. Petrol. Sci. Technol. 23 (2005) 749–760.
[49] C. López García, "Analyse de la réactivité des composes soufrés dans les coupes pétrolières: cinétique et modélisation de l'hydrotraitement", PhD Thesis, Claude Bernard Lyon I University, France, 2000.
[50] C. Moreau, P. Geneste, in: J. Moffat (Ed.), Theoretical Aspects of Heterogeneus Catalysis, 1990, New York.
[51] H.W. Wiser, et al. Ind. Eng. Chem. Prod. Res. Dev. 9 (1970) 350–357.
[52] C. Aubert, et al. J. Catal. 112 (1988) 12–20.
[53] A.V. Sapre, B.C. Gates, Ind. Eng. Chem. Process. Des. Dev. 20 (1981) 68–73.
[54] M. Nagai, T. Masunaga, Fuel 67 (1988) 771–774.
[55] M. Nagai, T. Miyao, S. Omi, 208th National Meeting American Chemical Society, vol. 36, Washington, (1994), pp. 577–583.
[56] S.C. Kim, F.E. Massoth, J. Catal. 189 (2000) 70–78.
[57] O. Bilous, N.R. Amundson, AIChE J. 2 (1956) 117–126.
[58] S. Vadja, H. Rabitz, Chem. Eng. Sci. 48 (1993) 2453–2461.
[59] J. Adler, J.W. Enig, Combust. Flame 8 (1964) 97–103.
[60] R.M. Chemburkar, et al. Chem. Eng. Sci. 41 (1986) 1647–1654.
[61] M. Morbidelli, A. Varma, Chem. Eng. Sci. 40 (1985) 2165–2168.
[62] M. Morbidelli, A. Varma, Chem. Eng. Sci. 44 (1989) 1675–1696.
[63] E. Bauman, et al. Chem. Eng. Sci. 45 (1990) 1301–1307.
[64] M. Morbidelli, A. Varma, AIChE J. 32 (1986) 297–306.
[65] M. Morbidelli, A. Varma, AIChE J. 33 (1987) 1949–1958.
[66] H. Wu, et al. Chem. Eng. Sci. 54 (1999), pp. 4579–4558.
[67] V. Balakotaiah, D. Luss, AIChE J. 37 (1991) 1780–1788.
[68] V. Balakotaiah, et al. Chem. Eng. Sci. 50 (1995) 1149–1171.
[69] E.L. Christoforatou, V. Balakotaiah, Chem. Eng. Sci. 52 (1997) 3463–3469.
[70] B. Marwaha, et al. Chem. Eng. Sci. 59 (2004) 5569–5574.
[71] M.A. Alós, et al. Chem. Eng. Sci. 51 (1996) 3089–3094.
[72] J.M. Zaldívar, et al. J. Loss Prevent. Proc. 16 (2003) 187–200.
[73] G.A. Viswanathan, D. Luss, AIChE J. 52 (2006) 1533–1538.
[74] G.A. Viswanathan, D. Luss, AIChE J. 52 (2006) 705–717.
[75] S. Surdarram, et al. AIChE J. 53 (2007) 1578–1590.
[76] G.F. Froment, K.B. Bischoff, Chemical Reactor Analysis and Design, John Wiley & Sons, 1990, pp. 376–391.
[77] D.D. Perlmutter, Stability of Chemical Reactors, Prentice-Hall Inc., New Jersey, 1972.